Melting by numbers: Assessing the effective melt fertility of crustal rocks

Jean-Louis Vigneresse, Bénédicte Cenki-Tok, Leo M Kriegsman

Journal Pre-proof

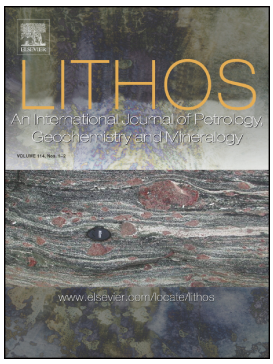

Melting by numbers: Assessing the effective melt fertility of crustal rocks

Jean-Louis Vigneresse, Bénédicte Cenki-Tok, Leo M. Kriegsman

PII: S0024-4937(21)00042-6

DOI: https://doi.org/10.1016/j.lithos.2021.106006

Reference: LITHOS 106006

To appear in: *LITHOS*

Received date: 28 October 2020

Revised date: 18 January 2021

Accepted date: 21 January 2021

Please cite this article as: J.-L. Vigneresse, B. Cenki-Tok and L.M. Kriegsman, Melting by numbers: Assessing the effective melt fertility of crustal rocks, *LITHOS* (2021), https://doi.org/10.1016/j.lithos.2021.106006

Melting by numbers: assessing the effective melt fertility of crustal rocks

Jean-Louis Vigneresse[1], Bénédicte Cenki-Tok[2], Leo M. Kriegsman[3]

[1]GéoRessources, UMR 7539, Université de Lorraine, 54506 Vandœuvre /Nancy Cédex, France, jean-louis.vigneresse@univ-lorraine.fr

[2]Géosciences Montpellier UMR5243, Université de Montpellier, CNRS, 34095 Montpellier cedex 5, France, benedicte.cenki-tok@umontpellier.fr

[3]Department of Research & Education, Naturalis Biodiversity Center, Darwinweg 2, 2333 CR, Leiden, the Netherlands, leo.kriegsman@naturalis.nl

ABSTRACT

Partial melting of rocks and the corresponding metamorphic reactions can be simulated through a Lagrangian description, which considers a discrete mineral distribution at sample scale and an infinite heat source. Our model aims to determine the effective melt productivity of crustal rocks linked to texture and composition of the source. In addition, it allows to assess the degree of melt fertility of greywackes and sandstones as a function of erosion and weathering of the source regions and of the tectonic environment in which the sediments were deposited. Our model is represented by a grid of cells, each containing a mineral phase or melt. The infinite heat source can be calibrated according to the melting equations. Melt extraction is ruled by the melt abundance in the source, and the melt sink is also an infinite reservoir. Our model presents three configurations each characterized by a specific melt fertility. Firstly, the spatial distribution of minerals can be random or anisotropic. Secondly,

the relative abundance of each mineral phase mimics the initial composition. Finally, the conditions of melt extraction reflect the tectonic environment in place when melt is extracted. The chemical reactivity is simply modelled from the equations of melting, yielding the maximum melt productivity as a function of reactants. The composition of the sediments is represented by a ternary diagram, built on quartz, micas and plagioclase. It mimics depositional environments issued from actual tectonic environments such as continental block erosion, continental basement reworking, or magmatic arc setting. Melting occurs when the effective bulk composition (or mineral assemblage) corresponds to the melting reaction stoichiometry. For a large range of sedimentary protoliths, the melt generated at the eutectic is of granitic composition. In other cases, optimum melt productivity cannot be reached, but the melt is removed when reaching a significant abundance. In other cases, such as an anisotropic mineral distribution, i.e. implying less chances to have the adequate minerals in contact, induces melt layering, similar to the one observed in stromatic migmatites. In order to enhance melt productivity and melt transfer, a deformation field is imposed to the model, mimicking simple or pure shear in a vertical plane, maintaining the 2D pattern of the model. Simple shear is efficient in bringing adequate minerals in contact and thus favors melt production. The source composition is examined using its average composition within a quartz-feldspars-lithic (QFL) diagram according to the origin of the sediments. Melt production from sediments resulting from continental basement reworking (e.g., arenites) is low (<< 10 % in volume), mostly because of the high quartz percentage. Sediments resulting from orogen recycling (e.g., argillites) also have a low melt productivity although mudstones can show melt productivity, up to 35-40 %. The only tectonic setting yielding a large amount of melt (> 40 %) corresponds to a magmatic arc setting. Such situations correspond to an enhanced extraction of the melt, through a horizontal lateral stress field, modelled by simple or pure shear in our experiments.

Keywords: metapelite dehydration, texture, protolith composition, melt productivity

Running title Melting by numbers

Submitted to Lithos

Version *1/27/2021*

Statistics words 10200 characters 68000 Figures 12

J.L. Vigneresse, GéoRessources, UMR 7539, Université de Lorraine, 54506 Vandoeuvre/Nancy Cédex, France

Tel 00 333 8368 4737 Fax 00 333 8368 4701

e-mail jean-louis.vigneresse@univ-lorraine.fr

Melting by numbers: assessing the effective melt fertility of crustal rocks

Jean-Louis Vigneresse[1], Bénédicte Cenki[2], Leo M. Kriegsman[3]

[1]GéoRessources, UMR 7539, Université de Lorraine, 54506 Vandœuvre /Nancy Cédex, France, jean-louis.vigneresse@univ-lorraine.fr

[2]Géosciences Montpellier UMR5243, Université de Montpellier, CNRS, 34095 Montpellier cedex 5, France, benedicte.cenki@umontpellier.fr

[3]Department of Research & Education, Naturalis Biodiversity Center, Darwinweg 2, 2333 CR, Leiden, the Netherlands, leo.kriegsman@naturalis.nl

ABSTRACT

Partial melting of rocks can be simulated through a Lagrangian description, which considers a discrete mineral distribution at sample scale and an infinite heat source. Our model aims to determine the effective melt productivity of crustal rocks linked to texture and composition of the source. In addition, it allows to assess the degree of melt fertility of greywackes and sandstones as a function of erosion and weathering of the source regions and of the tectonic environment in which the sediments were deposited. Our model is represented by a grid of cells, each containing a mineral phase or melt. The infinite heat source can be calibrated according to the melting equations. Melt extraction is ruled by the melt abundance in the source, and the melt sink is also an infinite reservoir. We tested three textural configurations, each characterized by a specific melt fertility. Firstly, the spatial distribution of minerals can be random or anisotropic. Secondly, the relative abundance of each mineral phase mimics the

initial composition. Finally, the conditions of melt extraction reflect the tectonic environment in place when melt is extracted. In order to address those three configurations, the chemical reactivity is simply modelled from the equations of melting, yielding the maximum melt productivity as a function of reactants. Melting occurs when the effective bulk composition (or mineral assemblage) corresponds to the melting reaction stoichiometry. This is an important constraint, different from PT modeling, in that sense that the model is not aimed to the composition, but to the effective fertility of the source. For a large range of sedimentary protoliths, the melt generated at the eutectic is of granitic composition. In other cases, optimum melt productivity cannot be reached, but the melt is removed when reaching a significant abundance. In other cases, such as an anisotropic mineral distribution, i.e. implying less chances to have the adequate minerals in contact, induces melt layering, similar to the one observed in stromatic migmatites. In order to enhance melt productivity and melt transfer, a deformation field is imposed to the model, mimicking simple or pure shear in a vertical plane, maintaining the 2D pattern of the model. Simple shear is efficient in bringing adequate minerals in contact and thus favors melt production. The composition of the sediments is represented by a ternary diagram, built on a quartz-feldspars-lithic (QFL) diagram. It mimics depositional environments issued from actual tectonic environments such as continental block erosion (CB), orogen recycling (OR), or magmatic arc (MA) setting. Melt production from sediments resulting from continental basement (CB) reworking (e.g., arenites) is low (<< 10 % in volume), mostly because of the high quartz percentage. Sediments resulting from orogen recycling (OR) (e.g., argillites) also have a low melt productivity although mudstones can show melt productivity, up to 35-40 %. The only tectonic setting yielding a large amount of melt (> 40 %) corresponds to a magmatic arc (MA) setting. We therefore suggest that the effective melt production from a former protolith rarely

overcomes 40 % as a very maximum, but more commonly less, and only in rare occasions reaches the 60 % from the melting reactions.

Keywords : metapelite dehydration; texture, effective melt productivity, protolith composition,

Running title Melting by numbers

Submitted to Lithos

Version *1/27/2021*

Statistics words 10200 characters 68000 Figures 12 Table 1

J.L. Vigneresse, GéoRessources, UMR 7359, Université de Lorraine, 54506 Vandoeuvre/Nancy Cédex, France

Tel 00 333 8368 4737 Fax 00 333 8368 4701

e-mail jean-louis.vigneresse@univ-lorraine.fr

Declaration of interest The present authors worked equivalently on the paper. JLV built the model and wrote the first draft with LMK. Many inputs and many improvements to the text and figures were provided by BC and JLV. They declare not having any commercial or associative interest that could represent conflicts of interest in connection with the present work.

Highlights

- A numerical estimate of melt in metapelites
- Effective melt productivity as a function of texture
- Effective melt productivity as a function of composition of the protolith
- Discontinuous melt extraction in spite of continuous heating

1. Introduction

Tectono-metamorphic processes controlling the bulk crustal evolution act as a combined effect of heat a granites. The melt production strongly differs, depending on the relative contribution of mantle and crustal processes on the earth's heat budget, but also according to the melting material. In addition, melting has a major influence on the rheology of the crust (e.g. Diener and Fagereng, 2014; Rey and Muller, 2010). In this context, understanding how the crust is able to produce melt is essential. Here, we explore, through a numerical model, the effective melt fertility of crustal rocks at sample scale looking at textures, and on a broader scale examining the protolith. It differs from other PT forward modeling (e.g. White et al., 2004 and following) in that we focus on physical processes and texture rather than chemical thermodynamic stability of melt-bearing assemblages.

Partially molten rocks occur as migmatites, that can be observed in many deeply eroded terranes. They provide natural examples of intermediate rocks between their metasedimentary source and leucogranitic magmas (Sawyer, 1998; Sawyer, 2020). Quartz, micas and plagioclases in the presence of water are among the first assemblages to produce melt in the range 650-850 °C. They correspond to sandstones, within the different poles between arkose, mudstone or siltstone, as defined in sedimentology. In metamorphic studies they are known as pelites, metapelites or greywackes. At low melt fraction, below ~10 vol.% in volume, isolated melt pockets are observed throughout the matrix (Holness, 1995; Vigneresse et al., 1996; Sawyer, 1998). At moderate melt fractions (~10-30 vol.%), melt pockets become interconnected, and migmatites are commonly banded with a leucocratic quartzo-feldspatic material, or leucosome, surrounded by two thin darker layers, or melanosome (Mehnert, 1968). Leucosome was often considered as the melt phase, yet crystallized and chemically

evolved from the primary melts, whereas the melanosome is commonly interpreted as the restitic part (e.g., Mehnert, 1968; Johannes, 1985). Recent developments (Stüwe, 1997; Kriegsman, 2001) and thermodynamic considerations (White et al., 2004; Mayne et al., 2019a) slightly modified this bimodal view, including retrograde reactions. The general aspect of migmatites is that of alternating layers of leucosome, mesosome (or paleosome) and melanosome. Incipient melt generation is controlled by the bulk distribution of minerals in the source rock and low melt fractions commonly mimic the original protolith texture (e.g. McLellan, 1988; Sawyer, 1998). However, with increasing melt fraction, and notably when assisted by deformation, melt is rapidly segregated, either into concordant veins (metatexites) or into discordant veins that disrupt the original layering (Vigneresse and Burg, 2004; Weinberg et al., 2013). Nevertheless, melt extraction during prograde reactions reduces fertility and increases the density and strength of residual crust (Yakymchuk and Brown, 2013; Mayne et al., 2019b, Clemens et al., 2020). Above ~30 vol.% melt, migmatites are considered as diatexites in which initial structures have lost their coherence (Mehnert, 1968; Sawyer, 1998). In the extreme range of pressure and temperature, with granulitic migmatite formation, the degree of partial melting may go up to 40 % (Morfin et al., 2013). Nevertheless, high degree of partial melting (above 50 %) may be observed in rocks where metric-scale cordierite cauliflower-like structures are present as restites within leucosomes (Barbey et al., 1999; Pawley et al., 2015). Such high degree of melting may go up to full melting when considering anatectic granites, in which some remnants of initial layering are more rarely observed.

The efforts have also focused on melting and melt extraction under the mid-oceanic ridges. But in such case, first the matrix is viscous, in contrast with a semi rigid migmatite, and second, the melt extraction is enhanced by external stress field. In consequence, numerical models are must easier to develop a representation of the interaction mantle-melt (Katz, 2008; Bo et al., 2018). Dynamics of partially molten assemblages in the crust (Schmelling et al.,

2019) has been addresses by purely physical numerical models involving two existing phase flow but does talke into account of melt inception processes.

Melting experiments provide information on the amount and chemical composition of the melt when th composition (e.g. water content) which may determine the total bulk melt fraction at each time (or temperature) step. However, the restricted volume of samples (a few cm^3 at most) is too small to investigate the influence of the textural distribution of minerals at sample scale. Furthermore, long experiments have to be run to approach equilibrium and several experiments are needed to investigate the respective role of each mineral phase. In addition, experiments optimize reactive conditions by using fine-grained and homogeneously mixed material, which deviates significantly from natural rocks.

The conditions of partial melting of metapelites, and the resulting characteristics of the melt produced, have been widely explored in the past decades since a thermodynamic model for haplogranitic melts has been implemented in consistent thermodynamic datasets (e.g. White et al., 2001). Upon temperature increase, hydrous minerals such as micas and amphiboles breakdown, yielding a melt of granitic composition (Fig. 1). Equilibrium forward thermodynamic modelling allows predicting stable mineral assemblages for a chosen local bulk composition (e.g. for review Lanari and Duesterhoeft, 2019). The role of equilibration domains in metamorphic processes is key to understand processes in highly heterogeneous rocks like migmatites (Guevara and Caddick, 2016). For example, the mechanisms of incipient partial melting and its effects on proto-leucosome composition and melt modal abundance, depending on melt dynamics has been widely explored since the seminal paper of White et al. (2004). Further models have then been refined recently for thermodynamic modelling of crustal melting (Connolly, 2004; Powell et al., 2018; Mayne et al., 2019b) The effects of multi-stage pelites melting and melt extraction on granulite mineral assemblages has also been characterized (Fornelli et al., 2002; Yakymchuk and Brown, 2013; Cenki-Tok et al.,

2016). The thermal consequences of melting for metapelites and granites have been quantified (Schorn, 2018), indicating that partially molten rocks form a thermal barrier to regional heat flow, owing to endothermic chemical reactions. The calculated fertility of these two protoliths differs by less than 7 % melt. However, these studies focus on the chemical and thermodynamic aspects of the melting/melt extraction processes leaving unexplored the associated physical mechanisms.

Macroscopic and microscopic observations on the distribution of incipient melting also provide information on where melt develops in a mineral assemblage. Incipient melting in pelitic rocks starts at triple or quadruple junctions between minerals of different species (Mehnert and Büsch, 1982). Under static equilibrium conditions, melt is commonly observed at grain boundaries of low activation energy, with specific dihedral angles controlling the shape of melt pockets in between grains (Laporte and Watson, 1995; Gleason et al., 1999). In some cases, the anisotropy of the crystalline network may alter this disposition (Wolf and Wyllie, 1991), but melt remains located in between grains boundaries, which are the most favorable sites in terms of chemical potential contrast. Those observations limited to thin section scale constitute a robust constraint on incipient melting and are essential when assessing the textural conditions of melting.

We have selected different stoichiometric reactions (Rushmer, 2001) after normalization to 1 muscovite and 1 biotite, adding the total molar melt percentage and the ratio melt/mole (Table 1). Globally the melt production is linear with 0.65 mole of melt normalized to 1 mole of reactant (Table 1). Investigations of static vs dynamic melt distribution as a function scale with a numerical model for partial melting at mineral assemblage scale. Field observations rarely record initial composition and mineral distribution before melting since the process of melting and melt loss drastically alters the protolith. Melting experiments and thermochemic approaches focus on thermodynamics, but rarely on stress and textural

disposition of minerals. In addition, they provide estimates of bulk melt production, but hardly consider melt productivity. We use a numerical code (Vigneresse and Burg, 2004) adopting one mineral grain for unit, integrating the chemical equations for melting and modal mineral abundance derived from field observations. Our model reproduces partial melting at sample scale depending on protolith composition and mineral distribution. We also introduce the concept and provide estimates of "effective melt fertility" for different metasedimentary rocks with modal compositions reflecting specific tectonic environments.

2. General assumptions for our models

The effective melt fertility of rocks depends on the modal abundance and distribution of minerals in the protolith. This dichotomic distribution has conducted to different views on partial melting. One is a purely naturalistic approach through sedimentology, experimental melting and the other is based on the principles of chemical thermodynamics.

2.1. Thermo-chemical framework for our models

Melting of metapelites occurs either when water is available, lowering the point of melting (Weinberg and Hasalová, 2015) or when hydrous minerals liberate water during dehydration melting (Clemens, 1990). In a simplified manner, the bulk rock chemistry of sediments can be modelled in NCK(FM)ASH system, implies that one does not distinguish between Fe and Mg. The acronym stands for Na_2O–CaO–K_2O–FeO–MgO–Al_2O_3–SiO_2–H_2O system (White et al., 2001). In parallel, several models of enhanced metamorphism yielding partial melting of metapelites have been developed in addition to the since the pioneering work of White et al. (2007), up to Powell et al. (2018) such as the Perple_X or Rcrust models (Connolly, 2005; Mayne et al., 2019b, Wang et al., 2019).

We use a set of equations similar to the NCKFMASH model, that encompassing more elements and are widely used up to pressure ranging 3000 MPa (Wei and Powell, 2006). This system, allows to represent reactions for metapelites, incorporating Ca, i.e. garnet, glaucophane, jadeite and omphacite. In the same range, amphibole dehydration is not considered, restricting the temperature below 800 °C and 1000 GPa (Gardien et al., 2000). The first liquid produced at 650 °C is Si-Al-K-rich containing low to null MgO, FeO, CaO, and Na_2O.A simple PT diagram shows the path, a synthetic prograde path (CW) starting at moderate pressure, still within the amphibolite facies, in preference to retrograde (CCW) paths (Fig. 1).

2.2. Experimental framework for our model

Most studies on experimental melting agree with the relative proportions of phases (Table 1) involved in muscovite dehydration melting (Harris et al., 1995). The modal abundance of the melt corresponds approximatively to the modal abundance of muscovite, with plagioclase and quartz in about equal proportion (Fig. 2). By contrast, the data set related to biotite dehydration melting indicates molar abundance varying by about 5 % between involved minerals as shown from a compilation (Rushmer, 2001) and experimental data (Patiño-Douce and Beard, 1995). We have also compiled other experiments (Le Breton and Thompson, 1988; Skjerlie and Johnston, 1992; Gardien et al., 1995). In our model, we neglect the volume change of the reactions.

Experimental melting considers ideal cases in which reactions stop when one of the reactants has been completely consumed (Fig. 2) In case of dehydration melting, micas, quartz and plagioclases need to be ideally mixed in stochiometric proportions, distributed evenly throughout a rock. No reactant ever becomes isolated from other reactants, and no

kinetic barriers exist that could hamper reaction progress, i.e. diffusion rates are infinite. It is approached in experimental petrology with very fine-grained and well mixed mineral samples. The resulting chemical fertility corresponds to the maximum amount of melt that can be produced from a given bulk rock chemistry. Hence 100% fertility is only realized when (i) minerals are distributed in equal proportion in stochiometric manner; and (ii) all minerals participate to the reaction; and (iii) no incongruent phase is produced. Dehydration melting of muscovite involves three minerals (quartz, plagioclase and muscovite), which have to be in contact with each other to produce melt. The reaction starts at about 720 ºC at 600 MPa, reaching 800 ºC at 900 MPa (Patiño-Douce and Harris, 1998). (Fig. 2).

Using volume coefficients, the reaction can be approximated as

$$1.0\ Ms + 0.4\ Qtz + 0.5\ Pl = 0.5\ Kfs + 0.4\ Sil + 1.0\ Melt \quad (1)$$

At higher temperatures (about 800-850 ºC), biotite dehydration melting produces garnet (or other incongruent phases such as cordierite and orthopyroxene) and melt. We have chosen garnet as the incongruent phase as it is the most common product in low-Mg metapelites at moderate pressures. The following balanced reaction, again using stoichiometric coefficients:

$$1.0\ Bt + 0.77\ Qtz + 0.35\ Sil + 0.85\ Pl = 1.0\ Grt + 0.27\ Kfs + 1.7\ Melt \quad (2)$$

Since their temperature stability fields do not overlap at moderate pressure (Fig. 3), both reactions may be combined into a single one that would operate over a larger temperature range, but with a melt production that is non-linear with temperature. Equating the sillimanite content in both equations and allowing it to drop out, gives:

$$1.0\ Ms + 1.14\ Bt + 1.28\ Qtz + 1.47\ Pl = 1.14\ Grt + 0.81\ Kfs + 2.94\ Melt \quad (3)$$

This gives an estimate of the bulk melt production for all bulk compositions. About 2.94 moles of melt are produced from 5 moles of reactants, thus yielding a ratio of 60 %, once a temperature of about 850 ºC has been reached. The fate of incongruent minerals, as expressed before, is not considered. An estimate for the amount not involved during melting. It is about equivalent to the amount of involved muscovite, thus representing less than 20 % in the bulk reaction muscovite plus biotite dehydration (Eq. 3) comes from the muscovite dehydration melting. Nevertheless, they represent about one third of the produced melt left as residual. Our limitation in temperature to 850 °C also imposes that no further reaction would produce melt. Similarly, the presence of amphiboles in the lithic part could increase the melt production. In our model, we used equations (1) and (2) consecutively, to examine the respective importance of each dehydration melting process in producing melt.

2.3. Sedimentological framework for our models

We consider the bulk rock composition of the protoliths in the simplified chemical system into three components, forming the QFL classification (Dickinson and Suczek, 1979; Dickinson, 1982; Weltje, 2002; Garzanti, 2019). The basic definition uses pure quartz (Q), feldspars (F) and lithic fragments (L). Because it has been designed for sediments, the term lithic shifted to rock fragments (R), may be more explicit (Weltje, 2002). Here we prefer considering L as other minerals other than quartz and plagioclases. In the original description (Dickinson and Suczek, 1979), lithic fragments encompass all sort of minerals. The point-counting method (Gazzi-Dickinson method) defines them as being in the sand-size fraction (<1 mm).

The classification of sedimentary rock types is represented in a ternary diagram (Fig. 4). Expressed in this system, the QFL classification contains the following end-member

minerals/phases. Garnet, appearing as incongruent phase during reactions, is assumed to be absent from the starting material.

$$\begin{aligned} &Q = Qtz \\ &F = Or, Ab, An \\ &L = Ms, Bt, Sil, Grt \end{aligned} \qquad (4)$$

The starting material is:

$$\begin{aligned} &Q_1 = Qtz \\ &F_1 = x\ Or + y\ Ab + (1 - x - y)\ An \\ &L_1 = a\ Ms + b\ Bt + (1 - a - b)\ Sil \end{aligned} \qquad (5)$$

It means that, when knowing the plotting positions in the QFL diagram (Fig. 4), there are still four variables (x, y, a, b) to deal with which have to be assigned arbitrary values.

Additional assumptions can be made to simplify the calculations. One assumption is to define a constant X_{An} of Pl, which is equal to the Ca/(Ca+Na) ratio of the melt. That means neglecting fractionation of Na and Ca, in agreement with sluggish diffusion in Pl (Johannes, 1985). In addition, it is assumed that Kfs = Or, i.e. there is no Ab component in Kfs. The system now simplifies to.

$$\begin{aligned} &Q_1 = Qtz \\ &F_1 = x\ Kfs + (1 - x)\ Pl \\ &\qquad [\text{where } Kfs = Or, \text{ and } 1\ Pl = X_{An}\ An + (1 - X_{An})\ Ab] \\ &L_1 = a\ Ms + b\ Bt + (1 - a - b)\ Sil \end{aligned} \qquad (6)$$

where a, b, x should be specified on the basis of additional data in the literature. Observations on medium-grade rocks also help to find reasonable values for these three

parameters. In most metapelites above 300 MPa, Kfs is absent before reaching muscovite dehydration melting. Hence, we assume that x = 0 (F_1= Pl) in metapelites. Psammites and greywackes, however, have considerable amounts of Kfs and often have similar compositions as granites. Hence, we assume x = 0.3 for such rocks. The lithic part of sediments reflects either their sedimen accordingly (Minami et al., 2016).

3. Modeling approach

The modeling is realized in two steps. We first identify the effect of specific textures, such as the layering or the disposition of minerals and the role of melt motion within the model. Then we address the compositional effect of the initial protolith, defined as a metasediment, but ranging from arenite, mudstone and sandstone according to the initial tectonic settings.

3.1 Model description, possibilities and limitations

Based on first order assumptions valid for thermo-geochemical modeling and experimental melting, we have built a numerical model to mimic the physical conditions of melting initiation and development at mineral scale. In addition, we address the textural effects of protolith sediments layering. We aim to determine an effective melting fertility for different compositions and texture of starting sedimentary rocks. The size of our models is intermediate between the mineral and outcrop scale.

The numerical code we use (Vigneresse and Burg, 2000; 2004) considers the evolution of the system (total melt percentage and distribution) at microscopic scale (or mineral/rock sample scale). The system is examined from the point of view of a particle, thus freeing of all parameters that have to be determined before a Eulerian notation is used (e.g. coordinates,

temperature, mass and momentum conservation). We illustrate both approaches (Vigneresse and Truche, 2020), with the example of a phase diagram (Fig. 5). The Eulerian description requires parameters such as temperature, melt viscosity, initial composition (A or B), and phase diagram (i.e. the curves determining the crystal/melt behavior as a function of temperature). It may also consider forming different crystal phases (M1 and M2). Only a global scale of melting can be examined and scaling for both time and temperature is sometimes problematic (Rabinowicz and Vigneresse, 2004). In contrast, the Lagrangian approach considers the physical state of a particle (i.e. its phase components, a liquid and crystals), the physical parameters (viscosity, temperature) are ignored. Time is addressed by the successive steps of running the numerical experiment, but there is no quantitative calibration. Temperature changes can be addressed by the progressive involvement of equations for muscovite, and biotite dehydration melting, but there is no direct quantitative calibration (Vigneresse and Burg, 2004).

The model consists in building a discrete grid of cells, arranged on a two dimensional (2D) hexagonal array in 64 * 38 lines and rows with periodic boundaries (Fig. 6). Each cell has a mineral scale (mm to cm, this is irrelevant). A large mineral, or a vein, will be represented by successive cells. During melting, each cell content may be replaced by product phases including melt. The model uses the chemical equations of dehydration (Eqs. 1 to 3) to control the modal evolution of the various phases. We have tested first a cubic distribution of minerals, but preferred an hexagonal distribution that implies a larger contact surface of a particle with its surrounding cells, enhancing the modal partition of elements (Fig. 6). The reactant minerals completely melt only if the surrounding cells reach the required proportions of all other mineral phases according to the stoichiometric melting equations (Eqs. 1 to 3). In addition, the hexagonal distribution allows a better representation of textures, such as layering or aggregates. The reaction may be incomplete if a given phase does not achieve the adequate

proportion. Depending on their spatial distribution, some cells cannot participate to melting because they are isolated or are not in contact with enough other mineral phases. The boundary conditions are periodic, i.e. when a cell from one side can be modified in its component by the adjacent cells on the other lateral boundary. In a first stage, the model is static, as it examines the occurrence of cells in the neighborhood and modifies their content according to dehydration equations.

An important constraint of the model is the absence of mafic component in the input material. The mantle component is totally absent by construction, either from is thermal inputs, initial and rejuvenation in temperature, but also in bringing mafic minerals contributing to the melt. Such limitation in the input parameters is inherent to the constructed model. It would have resulted in a large modification of the involved chemical reactions (Eqs. 1 to 3). The use of the dehydration melting equations, simply considering four mineral phases as inputs, also result in a unique melt composition. By the way, it is important to recall that the aim of the modeling is not to determine the chemical composition of the melt as a function of textures and source, but its amount.

Running the code in successive steps allows adding supplementary constraints that can mimic both temperature and time while both are not to scale. Temperature is the easiest to mimic in varying the initial melt percentage. Nevertheless, as imposed by the Lagrangian model, no calibration in temperature can be imposed. Dehydration proceeds first with muscovite dehydration melting at 700 °C, followed by biotite dehydration melting at about 760 °C (Fig. 1). Thus, the first equation is the rule during the first steps of the code, and after some steps, the second equation may occur. This should correspond to a very low amount or absence of muscovite in the effective local bulk (Stüwe, 1997. Time corresponds to the number of steps during which the reactions take place. It has also no scale. Reaction kinetics is by definition instantaneous in the model.

Furthermore, the introduction of steps in the model, as well as the periodic boundaries of the system allow testing addition dynamic properties of melting at sample scale (Fig. 6). Deformation, under pure and/or simple shear requires only shifting lines or rows (Fig. 6) according to the imposed strain pattern (Vigneresse and Burg, 2000; 2004). Translating cells enhances melting and increases melt productivity by allowing more mineral pairs to be in contact. The intensity of deformation may be tested by translating cell by one or several units, according to the deformation process chosen. Another dynamic disposition partitions deformation according to its composition. Melt being more mobile, its content may be moved accordingly toward adjacent cells. Melt motion depends on the thresholds, as the liquid percolation threshold (LPT) and the melt escape threshold (MET) previously identified (Vigneresse et al., 1996). Lateral motion of the melt is ruled by periodic boundaries. Melt escapes the cells as its amount overcomes MET but its vacancy is not replaced. It escapes in an infinite melt reservoir collecting the produced melt. Again, the Lagrangian description does not allow, and is not aimed at, predicting a structure or a geometry of the melt escape. The melt production requires an infinite heat source, in order to achieve the melting equations corresponding to the number of phases in contact. It corresponds to a varying degree of melting, mimicking heat pulses (increasing melt content) as transient situations in a more general manner (Fig. 6). The melt productivity is computed at each step as the quantity of melt extracted. It is then normalized to the size of the cell matrix. In a dynamic modeling, the normalization also incorporates the initial amount of melt yet present in the model.

3.2. Results of static modeling

The starting composition yielding optimum fertility consists in a mixture of Bt + Ms + Qtz and Pl (Eq. 1
(QFL) diagram introduced in sedimentary studies to describe sandstones, mudstone, and more

generally pelites (Dickinson, 1982). The ternary diagram certainly avoids considering the incongruent phases, either in the inputs or the ouptuts. It minimizes the amount of melt production by not considering their participation. But, their inherent incorporation into the lithic portion, and thus assimilating them to melting reactant balance the above quoted drawback.

The simplest model takes into account a random (Fig. 6r) disposition of minerals. The effective fertility is rarely higher than 50 %. In the other cases, minerals were distributed into layers representative of two categories of mineral (quartzo-feldspatic, or micas). When minerals were spatially organized within the layers (Fig. 6i), one mineral phase is concentrated into a domain or lens within each layer, the maximum length (i.e. the number of cells that form a continuous line) of which is constant (Fig. 6c). Our results document a fertility highly depending on initial textural arrangement of minerals. When minerals are arranged with a compositional layering (e.g. two layers, each being composed of quartzo-feldspatic phases or micas) inducing anisotropy, then melting preserves and amplifies the anisotropy, since the required minerals in contact do not correspond to the stoichiometry of melting reactions. The two textural dispositions create domains of inert minerals, that strongly reduce melting efficiency. Similarly, the thickness of the layers, measured in units of cells, was also explored. The melt fraction falls rapidly when the thickness of the layers increases (Fig. 7). Whereas fertility is around 25% for a one mineral cell thick layer, it falls to about 5% when the layer is 4 cells thick (Fig. 7). It becomes lower than 1% when the layer is 9 cells thick. Melting occurs at the interface between two layers, but it does not propagate inward, because of low diffusion rates.

Structures perpendicular or oblique to the initial mineral layering are observed only when the disposition of minerals presents adequate disposition (Fig. 6). Melt pockets develop at regular intervals in both the quartzo-feldspatic and the mica layers. But, due to the pseudo-

periodicity, those domains get connected developing an anisotropy perpendicular to the initial layering .

3.3. Results of dynamic modeling

In the previous setup, the global distribution of minerals remains static. A dynamic approach to melting in which strain redistributes the cell content, offers additional insights on the feedback loop between melting and deformation at sample scale. The dynamic model mimics pure shear or simple shear effects on minerals and melt distribution (Fig. 6). It is simulated by moving the cells to the adjacent one, along the largest stress component, thus equivalent to a strain rate (γ) of 1.

In nature, strain partitioning results in the segregation of the melt and formation of shear bands that alter the bulk response to the imposed stress pattern. The bulk distribution of solids is altered, leading to enhanced contacts between them, and thus modifying the possibility of reaching the appropriate optimum fertility. It thus implies a feedback loops between static melting and dynamic disposition of minerals.

The simultaneous effects of more mobile melt production at each step induces an irregular quantity of melt extracted at each step (Fig. 8). However, the coefficient of melt extraction, i.e. the quantity of melt extracted at each step multiplied by the initial amount of melt remains stable after a few steps (Fig. 8). It stabilizes as a function of the quantity of melt that can escape from the system or melt escape threshold (MET) (Vigneresse et al., 1996). The irregular melt productivity is a combination of two factors. First, the quantity of melt produced at each step is highly dependent of the initial melt availability relative to the MET. A too large initial melt percentage cannot be evacuated from the system and reach a steady

state. Similarly, a low initial MET results in a deficiency in extraction. Both form stiction spikes (Fig. 8). Similarly, if a sudden increase in melt productivity occurs, as for instance when biotite dehydration melting starts, resulting in an increase in melt productivity, a stiction spikes occurs that needs some steps before returning to a steady state. Secondly, irregular melt production due to the variable number of particles in contact may produce small variations analogue to stick-slip motion during friction (Burridge and Knopoff, 1967).

The effect of strain during melting is more affected by the amount of melt than by the amount of stress, whatever it is pure or simple shear (Fig. 9). Pure shear, i.e. shortening, is more effective in expulsing the melt from its matrix, compared to simple shear that simply displaces the melt by strain partitioning, but puts in contact other groups of minerals, thus enhancing melting. Although the effect of strain partitioning could be taken into account by moving the melt cells faster than minerals cells, it remains difficult to amplify the anisotropy in the melt/solid distribution. However, this observation may also result from a 2D geometrical artifact of the modelling since simple shear displace the melt laterally, i.e. toward periodic boundaries, thus without escaping the model.

4. Crustal fertility and geodynamic settings

Continental basement erosion (CB), fluvial orogen recycling (OR), as well as volcanic and plutonic products in magmatic arc (MA) define three general categories of sediments that are potential source of further reworking and melting (Dickinson, 1982; Garzanti, 2019, Fig. 4). The two first categories correspond to eolian and fluvial erosion of continental protolith. At first order, these processes occur on passive margins. The third category includes volcanic and plutonic products that rather form in active margins.

The three categories include a large variety of sediments ranging in bulk from arkoses, argilites and mudstones (Fig. 10). Continental eolian sediments (CB) are from the Older and Lower Red Sandstones from England (Hillier et al., 2006) and from the Tarim Basin, China (Rittner et al., 2016) and Turkey (Löwen et al., 2018). They are characterised by a relative abundance of quartz, with few micas, but K-feldspars. Consequently, a poor effective melt productivity is expected. Sediments from large rivers and marginal basins (OR), have been compiled (e.g. Weltje, 2002; Garzanti, 2019) from the East and West Pacific active margins as well as from the Atlantic, Indian Ocean and Mediterranean passive margins. The sediments record the complete evolution from the collisional stage and high elevation mountain uplift followed by fluvial erosion. Sedimentation evolves from sandstones and metapelitic detritus to more mature sediments with abundant mudstone. The Pacific margins show a progressive evolution indicating the evolution of the magmatic arcs (MA) that progressively starts from plutonic detritus from the arc basement, both equally rich in quartz and feldspars (Garzanti, 2019). Then, depending on the fate of the arc, undissected arcs sediments shift to quartz-poor sediments and increase in biotite, reflecting the volcanic settings. Pure volcanic environments show no quartz at all and more than 50 % of micas with respect to feldspars. Transitional and dissected arcs are intermediate between arc basement and the lithic pole. Quartz abundance decreases from about 50 to15 %, whereas feldspars abundance remains constant. Micas slightly increase, indicating the ongoing volcanic activity (Maynard et al., 1982; Weltje, 2012). Their content, always quartz-poor, but increases upwards from <1% to an average ranging 5 to 10%, with a maximum of 15 %. Lithic fragments are exclusively volcanic, strongly dominant over feldspars. The latter are invariably plagioclases (8 to 17 %), presently albitized.

Refining the contents of plagioclases and lithic fragments (Fig. 11), it is possible to infer the average melt productivity in the three generic settings, i.e. composition, represented

by sandstones. An average melting path, with an average compositional range is estimated for the three situations (CB, OR, MA). It defines the bulk composition in each setting, but because the domain extends wider than the path, some lateral extensions are selected that widen the productivity within each domain. In addition, the mineral content is adapted from the ternary QFL diagram, and further refined for each component (Fig. 11). Four groups of minerals, namely plagioclase, K-feldspar, biotite and muscovite are identified. Their respective abundance is reported in our model of numerical melting. We use several textural combinations, from random to layered (Fig. 6), with two end-members depending on the layer thickness as in the generic model (Fig. 7). The thick layer model shows a lower melt productivity, as expected, hardly reaching a total of 28 %. Alternatively, a thin layer model shows a more or less concentric disposition, reaching 65 % of melt towards the lithic components, i.e. larger muscovite and biotite amount. This makes sense since they are the major minerals involved in the considered dehydration melting reactions, progressively increasing from 3 to 15 % .

As expected eolian sediments (CB) show a low melt productivity (3 to 10 %), reflecting the elevated quartz amount. Dismembered orogens (OR) present in a variable effective melt productivity, ranging up to 40% in case of progressive enrichment in mudstone, as in the case of fluvial sediments pouring into the Indian Ocean. However, the melt productivity, averaging 20-30 %, is controlled by the quartz abundance that progressively decreases from 95 to 50 % (Fig. 12). The case of magmatic arc (MA) with a mineral evolution richer in micas presents an effective melt Ingersoll, 1992). The effective melt productivity even shows maximum values, close to 40 % when approaching the ideal composition at which quartz and feldspars are in nearly equal proportion with the two micas (Eq. 3).

5. Melt composition

The melt composition is essentially controlled by the melting equation, i.e. its stoichiometric components. Consequently, varying the relative proportion of elements affects the amount of the melt, but not its composition. The result, as stated during the experiments is a melt of granitic composition (Gardien et al., 1995).

To address variation in the melt composition requires changing the equations of melting or adopting a numerical code of enhanced metamorphism such as Perple_X (Connolly, 2009) or Rcrust (Mayne et al., 2016). It supposes also incorporating alumino-silicate minerals (e.g. sillimanite, garnet or cordierite not considered in priority here.

6. Effective melt productivity/fertility?

The effective melt fertility explored through numerical modeling here allows bracketing what is observed on the field and in several tectonic conditions. Indeed, the low effective melt productivity in some metasediments contrasts with some migmatitic areas, whatever the loss of extracted melt, as previously described, for example in Finland by J.J. Selderholm, (Eklund et al., 2008).

6.1. Crustal fertility

The maximum melt productivity is 55 % for the mineral assemblage Ms + Bt + Qtz + Pl with mineral abundances corresponding to the reaction stoichiometry (Gardien et al., 1995). The value falls to 50% when about 10 vol % of an inert phase is introduced, and it is about 40

% when the amount of inert phase (e.g. K-feldspar) equals the amount of plagioclase or when the exact composition departs by about 20 % from the ideal stoichiometric composition.

If K-feldspar is considered as an inert or non-reactive phase in some cases, this has direct implications for crustal fertility, since it is ubiquitously present in crustal rocks. In addition, retrograde reactions between minerals and melt may also occur, leading to segregation into melt-rich and restitic domains. Back reactions may also locally develop between melt and restites (Stüwe, 1997; Kriegsman, 2001, Cenki et al., 2002). If the melt sits where it has been created upon cooling then some components of the melt (usually Pl or Qtz) can react during melt-consuming reactions (or backreactions) and Kfs is left behind, altering the reactive bulk domain.

Actual estimates refer to about 5% in the bulk crust, but 20% in the upper crust (Taylor and McLennan, 1995). Hence, K-feldspar may act as a damping factor during dehydration melting reactions. Crustal material may become enriched in such inert by-products of dehydration melting reactions during successive orogenic stages which could contribute to lower subsequent melt productivity. Inert phases may thus act as a stabilizing factor in crustal evolution generating refractory domains (Dhuime et al., 2018). Highly refractory composition may be generated as well during successive events of melting allowing rocks to attain ultra-high temperatures without melting (Cenki-Tok et al., 2016). Nevertheless, the origin of sediments that later are involved in melting the continental crust are of primary importance in generating an effective melt productivity. In particular there is a strong difference in crustal fertility between subduction and collision related margins (Moyen et al., 2017).

Although it incorporates a static and a dynamic behavior, our model cannot assess the evolution of the melt composition as a function of melt extraction (Mayne et al., 2019). This is the consequence from the initial condition of an infinite reservoir for the source and melt

sink. Hence melt extraction, though its amount is quantified and demonstrate a discontinuous behavior (Fig. 8) may modify the contact between grains, thus modifying the necessary contact between minerals that are involved in the melting reaction. Two extreme situations may thus result from a different mode of melt extraction. In the less favorable case, i.e. no melt extraction at all, the melt acts as an inert phase that prevents the contact between minerals. It would rapidly generate a brutal decrease in melt production, unless retrograde reactions remove some amount of melt, establishing new contacts between adequate minerals. The other extreme situation is the immediate removal of the melt, whatever the equivalent porosity of the source is. It enhances further contacts between appropriate minerals and would increase melt production but not necessarily alter the optimum melt production. In both cases, the extraction of the melt is linked to the surrounding stress pattern, that may activate or not melt removal. Such situations correspond to the distinction between usual migmatites and diatexites (Mehnert, 1968; Sawyer, 1998).

6.2. Comparison with migmatitic terranes

In the field, migmatites (Fig. 1) are usually separated in categories taking into account their temperature, e.g. degree of partial melting, pressure conditions, e.g. depth of formation and protolith composition (e.g. Sawyer, 2008). The temperature of melting ranges from 650°C, the onset of water-assisted muscovite dehydration, up to nearly 900 °C with granulite formation. The amount of melt may be very low, as simple unconnected melt pockets, i.e. < 5%vol, as observed in low temperature metasediments from Namibia for example (Ward et al., 2008). Diatexites are estimated to have more than 12-20 % melt and their original texture is obliterated (Sawyer, 1998).

Nevertheless, the exact quantity of melt present in migmatites remains difficult to estimate. Firstly, the amount of extracted melt can hardly be restored. Secondly, back-reactions during crystallization obscure the geochemical signatures recorded during equilibrium or disequilibrium melting (Kriegsman, 2001). In particular, trace element distribution between leucosome and host rock cannot be used to infer melt segregation rates (Nyström and Kriegsman, 2003). Indeed, the slopes (dP/dT) of most dehydration reactions steepen considerably with melting (Fig. 1). The application of classical thermobarometers involving only solid phases (e.g. Grt-Opx-Pl-Qtz) to unravel the P-T evolution of anatectic migmatites, in which melt is omnipresent, may be problematic (Cenki et al., 2002).

In conclusion, the exact melt quantity present in migmatites is difficult to evaluate, though melt extraction is not always efficient. The takeaway message that could be formulated from the present modeling and from field observations is, surprisingly, not linked to the melt amount. Hence, the present paper considers endothermic melting in various original compositions of the protolith, leaving some amount of restitic material. But it lacks considering the fate of such incongruent minerals, the same way it lacks considering exothermic retrograde reactions. Both effects induce a buffering effect in the reactions, implying a temperature damping, excluding too high temperature (Depine et al., 2008).

In contrast, granulitic terranes (Fig. 1) are commonly considered as the restitic phases after dehydration melting (Clemens, 1990). However, fluid-present granulites are interpreted as being formed by relatively low-temperature, above 650 °C, dehydration melting reactions. Non-restitic, mafic granulites or so called charnockites represent basaltic magma that may provide the heat source for metamorphism and melting of the overlying rocks. In contrast, fluid-absent granulites produced at temperature above 850°C, may be coeval with the formation of voluminous granitoids or the result of a series of melting/extraction events. Such restitic granulites are the residual complements, or refractory material, of felsic

magmas that have moved to higher levels (Clemens, 1990). As an example, a mass balance for the melt-depletion in granulite terrane of Ashuanipi subprovince, Quebec indicates extraction of between 20 and 40 wt %, granitic melt (Guernina and Sawyer, 2003).

6.3. Dehydration reactions

The suggested mechanism of melting through micas dehydration melting enters the global process of progressive loss of water, or hydroxyls with temperature. The volume of liberated fluids is not continuous, as suggested by our numerical modelling of melt extraction (Fig. 8). The alternating jumps in amount of fluid are similar to stick-slip motion during friction (Burridge and Knopoff, 1967), suggesting instability development dues to the contrasted rheology of the fluid in its matrix. The liberated fluids alter the local pore fluid (Dobson et al., 2002; Tarling et al., 2019), with the possibility of inducing earthquakes, and even so-called silent earthquakes (Im et al., 2020).

Such discontinuous motions relate to the hysteretic nature of friction, implying that some additional energy is required to return to the initial state, proceeding from the fact that dehydration reactions are endothermic (Schorn et al., 2018), absorbing heat during reactions. It represents the thermo-chemical aspects of dehydration. But such reactions also imply the switch from a one mechanical phase (solid crystals) to a two-phase system (solid + fluid), thus having mechanical impacts on the rheology of the system. The consequence is a switch from continuous reactions due to heat toward a discontinuous mechanical response.

6.4. Melt fertility in different tectonic settings

The models performed for different mineral compositions highlight the enhanced fertility of magmatic arcs (MA) compared to the very low melt production in case of eolian erosion (CB) (Fig. 12). Fluvial transport of sediments (OR) is highly dependent on the dimension of the drainage basin and on its average elevation It has implication on crustal reworking, and especially in new crust generation at plate boundaries. The topic has been addressed in several ways, mostly using isotopic studies and detrital zircons (Armstrong, 1991; Taylor and McLennan, 1985). They both converge to show that the production of juvenile continental crust is presently balanced by recycling with a peat change at about 3.0 Ga, assuming that about 65 % of the continental crust existed at that time (Dhuime et al., 2012).

The remaining possibility for recycling a felsic crust is through active margins, provided that the contin crustal lithologies (Collins, 2002), especially during hot orogenies (Clemens, 2003; Miller et al., 2003). The change of convergence velocity, linked to slab retreat and back-arc opening, may favour heat upwelling from the mantle, leading to intense melting of arc-derived material (MA).

7. Conclusions

Our physico-chemical model of melting is, to our knowledge, a first attempt to quantify crustal fertility at sample scale according to the initial mineral assemblage and rock fabric. We have therefore introduced the term of “effective fertility” as the average amount of melt produced in various environments that may be identified for crustal recycling. Such results include a static and a dynamic modeling of metasediments resulting from eolian,

fluvial erosion and magmatic arc activity. The former setting is by the far the less productive (<<10 vol %) due to its large abundance of quartz over other mineral phases. Fluvial erosion involves more mudstone and therefore an enhanced melt productivity (20-30 %). Magmatic arcs represent a good candidate for renewed melting, i.e. high crustal fertility, since their sedimentary sequence involves a significant amount of micas. The effective melt productivity averages about 40 vol%. The effective fertility of some source rocks, depending on domain texture and modal composition, is generally significantly lower than the bulk fertility estimated only from the bulk percentage of mineral phases. Consequently, it implies that models for crustal derived magma production involve more material than previously estimated for their source.

Acknowledgements

The authors wish to thank Annika Nyström (former PhD researcher at Turku University 1999-2003) for literature research on sedimentary data. JLV acknowledges a travel and lodging grant (Spring 2000) from the Turku University Foundation. LMK has benefited from research grant 68645 for the years 2000 and 2001 by the Finnish Academy. BC acknowledges the funding from the European Union's Horizon 2020 research and innovation program under grant agreement No 793978. We also acknowledge the constructive comments of the two reviewers, including Matt Mayne (Stellenbosch U., RSA).

REFERENCES

Armstrong, R.L., 1991. The persistent myth of crustal growth. *Australian Journal of Earth Sciences* 38, 613–630. doi:10.1080/08120099108727995

Barbey, P., Marignac, C., Montel, J.M., Macaudière, J., Gasquet, D., Jabbori, J., 1999. Cordierite growth textures and the conditions of genesis and emplacement of crustal granitic magmas; the Velay granite complex (Massif Central, France). *Journal of Petrology* 40, 1425-1441. doi:10.1093/petroj/40.9.1425

Bo, T., Katz, R. F., Shorttle, O., Rudge, J. F. 2018. The melting column as a filter of mantle trace-element heterogeneity. *Geochemistry, Geophysics, Geosystems* 19, 4694–4721. doi:10.1029/2018GC007880

Burridge, R., Knopoff, L., 1967. Model and Theoretical seismicity. B*ulletin of the Seismological Society of America* 57, 341-371.

Cenki, B., Kriegsman, L.M., Braun, I., 2002. Melt-producing and melt-consuming reactions in anatectic granulites: P–T evolution of the Achankovil cordierite gneisses, South India. *Journal of Metamorphic Geology* 20, 543-561. doi:10.1046/j.1525-1314.2002.00388.x

Cenki-Tok, B., Berger, A., Gueydan, F., 2016. Formation and preservation of biotite-rich microdomains in high temperature rocks from the Antananarivo Block, Madagascar. *International Journal of Earth Sciences* 105, 1471-1483. doi:10.1007/s00531-015-1265-0

Clemens, J.D., 1990. The granulite-granite connexion. In: Vielzeuf, D., Vidal, P. (Eds) *Granulites and Crustal Evolution*. NATO ASI Series C, 311. Springer, Dordrecht. 25-36. doi:10.1007/978-94-009-2035-2_3

Clemens, J.D., 2003. S-type granitic magmas - petrogenetic issues, models and evidence. *Earth Science Reviews* 61, 1-18. doi:10.1016/S0012-8252(02)00107-1

Clemens, J.D., Stevens, G., Bryan S.E., 2020. Conditions during the formation of granitic magmas by crustal melting – Hot or cold; drenched, damp or dry? Earth-Science Reviews 200, 102982. doi:10.1016/j.earscirev.2019.102982

Collins, W.J., 2002. Hot orogens, tectonic switching, and creation of continental crust. *Geology* 30, 535-538. doi:10.1130/0091-7613(2002)030<0535:HOTSAC>2.0.CO;2

Connolly, J.A.D., 2005. Computation of phase equilibria by linear programming: A tool for geodynamic modeling and its application to subduction zone decarbonation. Earth and Planetary Science Letters 236, 524-541. doi:10.1016/j.epsl.2005.04.033

Connolly, J.A.D., 2009. The geodynamic equation of state: what and how. *Geochemistry, Geophysics, Geosystems* 10, Q10014. doi:10.1029/2009GC002540

Depine, G.V., Andronicos, C.L., Phipps-Morgan, J., 2008, Near-isothermal conditions in the middle and lower crust induced by melt migration. *Nature* 452, 80-83. doi:10.1038/nature06689

Dhuime, B., Hawkesworth, C.J., Cawood, P.A., Storey, C.D., 2012. A change in the geodynamics of continental growth 3 billion years ago. *Science* 335, 1334-1336. doi:10.1126/science.1216066

Dhuime, B., Hawkesworth, C.J., Delavault, H., Cawood, P.A., 2018. Rates of generation and destruction of the continental crust: implications for continental growth. *Philosophical Transactions of the Royal Society* A376, 20170403. doi:10.1098/rsta.2017.0403

Dickinson, W.R., 1982. Composition of sandstones in Circum-Pacific subduction complexes and fore-arc basins. *AAPG Bulletin* 66, 121-137.

Dickinson, W.R., Suczek, C.A., 1979. Plate tectonics and sandstone composition. *AAPG Bulletin* 63, 2164-2182. doi:10.1306/2F9188FB-16CE-11D7-8645000102C1865D

Diener, J.F.A., Fagereng, Å., 2014. The influence of melting and melt drainage on crustal rheology during orogenesis. *Journal of Geophysical Research* B119, 6193-6210. doi:10.1002/2014JB011088

Dobson, D.P., Meredith, P.G., Boon, S.A., 2002. Simulation of subduction zone seismicity by dehydration of serpentine. *Science* 298, 1407–1410. doi:10.1126/science.1075390

Eklund, O., Vaïsanen, M., Ehlers, K., Kousunen, P., Kurhila, M., Lehtinen, M., Sorjonen-Ward, P., 2008. 100 years of migmatite - In Sederholms footsteps. *33 IGC excursion No 16*, 40 pp. http://www.33igc.org/filesshare/filArkivRoot/coco/FieldGuides/No%2016%20Sederholms%20foot%20steps.pdf

Fornelli, A., Ornelli, G., Piccarreta, G., Del Moro, A., Acquafredda, P., 2002. Multi-stage Melting in the Lower Crust of the Serre (Southern Italy), *Journal of Petrology* 43, 2191–2217, doi:10.1093/petrology/43.12.2191

Gardien, V., Thompson, A.B., Grujic, C., Ulmer, P., 1995. Experimental melting of biotite + plagioclase ± muscovite assemblages and implications for crustal melting. *Journal of Geophysical Research* B100, 15581-15591. doi:10.1029/95JB00916

Gardien, V., Thompson, A.B., Ulmer, P., 2000. Melting of biotite + plagioclase + quartz gneisses: the role of H_2O in the stability of amphibole. *Journal of Petrology* 41, 651-666. doi:10.1093/petrology/41.5.651

Garzanti, E., 2019, Petrographic classification of sand and sandstone. *Earth-Science Reviews* 192, 545-563. doi:10.1016/j.earscirev.2018.12.014

Gleason, G.C., Bruce, C., Green, H.W., 1999. Experimental investigation of melt topology in partially molten quartzo-feldspathic aggregates under hydrostatic and non-hydrostatic stress. *Journal of Metamorphic Geology* 17, 705-722.

Guernina, S., Sawyer, E.W., 2003. Large-scale melt-depletion in granulite terranes: An example from the Archean Ashuanipi subprovince of Quebec. *Journal of Metamorphic Geology* 21, 181-201. doi:10.1046/j.1525-1314.2003.00436.x

Harris, N., Ayres, M., Massey, J., 1995. Geochemistry of granitic melts produced during the incongruent melting of muscovite: Implications for the extraction of Himalaya leucogranite magmas. *Journal of Geophysical Research* B100, 15767-15777. doi:10.1029/94JB02623

Hillier, S., Wilson, M.J., Merriman, R.J., 2006. Clay mineralogy of the Old Red Sandstone and Devonian sedimentary rocks of Wales, Scotland and England. *Clay Minerals* 41, 433-471. doi:10.1180/0009855064110203

Holness, M.B., 1995. The effect of feldspar on quartz-H_2O-CO_2 dihedral angles at 4 kbar, with consequences for the behaviour of aqueous fluids in migmatites. *Contributions to Mineralogy and Petrology* 118, 356-364. doi:10.1007/s004100050020

Im, K., Saffer, D., Marone, C., Avouac, J.P., 2020. Slip-rate-dependent friction as a universal mechanism for slow slip events. *Nature Geoscience* 13, 1-6. doi:10.1038/s41561-020-0627-9

Johannes, W., 1985. The significance of experimental studies for the formation of migmatites. In: Ashworth, J.R. (ed), *Migmatites*, Blackie, Glasgow, 36-85. doi:10.1007/978-1-4613-2347-1_2

Johannes, W., Holtz, F., 1996. *Petrogenesis and Experimental Petrology of Granitic Rocks*. Springer Verlag, Heidelberg, 340 pp. doi:10.1007/978-3-642-61049-3_9

Katz, R.F., 2008. Magma dynamics with the enthalpy Method: Benchmark Solutions and Magmatic Focusing at Mid-ocean Ridges, *Journal of Petrology* 49, 2099–2121. doi:10.1093/petrology/egn058

Kriegsman, L.M., 2001. Partial melting, partial melt extraction, and partial back reaction in anatectic migmatites. *Lithos* 56, 75-96. doi:10.1016/S0024-4937(00)00060-8

Kriegsman, L.M., Nyström, A.I., 2003. Melt segregation rates in migmatites: review and critique of common approaches. In: Vance, D., Müller, W., Villa, I.M. (Eds). *Geochronology: Linking the Isotopic Record with Petrology and Textures*. Geological

Society of London, Special Publications 220, 203-212. doi:10.1144/GSL.SP.2003.220.01.12

Lanari, P., Duesterhoeft, E., 2019. Modeling metamorphic rocks using equilibrium thermodynamics and internally consistent databases: Past achievements, problems and perspectives. *Journal of Petrology* 60, 19-56. doi:10.1093/petrology/egy105

Laporte, D., Watson, E.B., 1995. Experimental and theoretical constraints on melt distribution in crustal sources: the effect of crystalline anisotropy on melt interconnectivity. *Chemical Geology* 124, 161-184. doi:10.1016/0009-2541(95)00052-N

LeBreton, N., Thompson, A.B., 1988. Fluid-absent (dehydration) melting of biotite in metapelites in the early stages of crustal anatexis. *Contributions to Mineralogy and Petrology* 99, 226-237. doi:10.1007/BF00371463

Löwen, K., Meinhold, G., Güngör, T., 2018. Provenance and tectonic setting of Carboniferous–Triassic sandstones from the Karaburun Peninsula, western Turkey: A multi-method approach with implications for the Palaeotethys evolution. *Sedimentary Geology* 375, 232-255. doi:10.1016/j.sedgeo.2017.11.006

Lundberg, N., 1991. Detrital record of the early Central American magmatic arc: Petrography of intraoceanic forearc sandstones, Nicoya Peninsula, Costa Rica. *Geological Society of America Bulletin* 103, 905-915. doi:10.1130/0016-7606(1991)103<0905:DROTEC>2.3.CO;2

Marsaglia, K.M., Ingersoll, R.V., 1992. Compositional trends in arc-related, deep-marine sand and sandstone: A reassessment of magmatic-arc provenance. *Geological Society of America Bulletin* 104, 1637-1649. doi:10.1130/0016-7606(1992)104<1637:CTIARD>2.3.CO;2

Maynard, J.B., Valloni, R., Yu, H.S., 1982. Composition of modern deep-sea sands from arc-related basins. In: Legget, J.K. (Ed.), *Trench-Forearc Geology: Sedimentation and Tectonics on Modern and Ancient Active Plate Margins*. Geological Society of America Special Paper 284, 21-40. doi:10.1144/GSL.SP.1982.010.01.36

Mayne, M.J., Moyen, J.F., Stevens, G., 2019. A phase equilibrium investigation of selected source controls on the composition of melt batches generated by sequential melting of an average metapelite. In: Janoušek, V., Bonin, B., Collins, W.J., Farina, F., Bowden, P. (Eds), *Post-Archean Granitic Rocks: Petrogenetic Processes and Tectonic Environments*. Geological Society of London, Special Publication 491, 223-241. doi:10.1144/SP491-2018-121

Mayne, M.J., Moyen, J.F., Stevens, G., Kaislaniemi, L., 2016. Rcrust: a tool for calculating path-dependent open system processes and application to melt loss. *Journal of Metamorphic Geology* 34, 663-682. doi:10.1111/jmg.12199

Mayne, M.J., Stevens, G., Moyen, J.F., 2019b. A phase equilibrium investigation of selected source controls on the composition of melt batches generated by sequential melting of an average metapelite. In: Janoušek, V., Bonin, B., Collins, W.J., Farina, F., Bowen, P. (Eds).*Post-Archean Granitic Rocks: Petrogenetic Processes and Tectonic Environments.* Geological Society, London, Special Publications 491, 223-241. https//doi.org/10.1144/SP491-2018-121

Mayne, M.J., Stevens, G., Moyen, J.F., Johnson, T., 2019a. Performing process-oriented investigations involving mass transfer using Rcrust: a new phase equilibrium modelling tool. In: Janoušek, V., Bonin, B., Collins, W.J., Farina, F., Bowen, P. (Eds).*Post-Archean Granitic Rocks: Petrogenetic Processes and Tectonic Environments.* Geological Society, London, Special Publications 491, 209-221 https://doi.org/10.1144/SP491-2018-85

McLellan, E.L., 1988. Migmatite structures in the Central Gneiss Complex, Boca de Quadra, Alaska. *Journal of Metamorphic Geology* 6, 517-542. doi:10.1111/j.1525-1314.1988.tb00437.x

Mehnert, K.R., 1968. *Migmatites and the Origin of Granitic Rocks*. Elsevier, Amsterdam, 400 pp.

Mehnert, K.R., Büsch, W., 1982. The initial stage of migmatite formation. *Neues Jahrbuch für Mineralogie Abhandlungen.* 145, 211-238.

Miller, C.F., McDowell, S.M., Mapes, R.W., 2003. Hot and cold granites? Implications of zircon saturation temperatures and preservation of inheritance. *Geology* 31, 529-532. doi:10.1130/0091-7613(2003)031<0529:HACGIO>2.0.

Minami, Y., Imura, T., Hayashi, S., Ohba, T., 2016. Mineralogical study on volcanic ash of the eruption on September 27, 2014 at Ontake volcano, central Japan: correlation with porphyry copper systems. *Earth Planet and Space* 68, 67 https://doi.org/s40623-016-0440-2

Morfin, S., Sawyer, E.W., Bandyayera, D., 2013. Large volumes of anatectic melt retained in granulite facies migmatites: An injection complex in northern Quebec. *Lithos* 168-169, 200-218. doi:10.1016/j.lithos.2013.02.007

Moyen, J.F., Laurent, O., Chelle-Michou, C., Couzinié, S., Vanderhaeghe, O., Zeh, A., Villaros, A., Gardien, V., 2017. Collision vs. subduction-related magmatism: Two

contrasting ways of granite formation and implications for crustal growth. Lithos 277, 154-177. doi:10.1016/j.lithos.2016.09.018

Nyström, A.I., Kriegsman, L.M., 2003. Prograde and retrograde reactions, garnet zoning patterns, and accessory phase behaviour in SW Finland migmatites, with implications for geochronology. In: Vance, D., Müller, W., Villa, I.M. (Eds). *Geochronology: Linking the Isotopic Record with Petrology and Textures*. Geological Society of London, Special Publications 220, 213-230. doi:10.1144/GSL.SP.2003.220.01.13

Patiño-Douce, A.E., 1999. What do experiments tell us about the relative contributions of crust and mantle to the origin of granitic magmas? In: Castro, A., Fernandez, C. and Vigneresse, J.L. (Eds), *Understanding Granites: Integrating New and Classical Techniques*. Geological Society of London, Special Publication 168, 55-75. https://dx.doi.org/10.1144/GSL.SP.1999.168.01.05

Patiño-Douce, A.E., Beard, J.S., 1995. Dehydration-melting of biotite gneiss and quartz amphibolite from 3 to 15 kbar. *Journal of Petrology* 36, 707-738. doi:10.1093/petrology/36.3.707

Patiño-Douce, A.E., Harris, N., 1998. Experimental constraints on Himalayan anatexis. *Journal of Petrology* 39, 689-710. doi:10.1093/petroj/39.4.689

Pawley, M., Reid, A., Dutch, R., Preiss, W., 2015. Demystifying migmatites: introduction for field-based geologist. *Applied Earth Science Transactions of the Institutions of Mining and Metallurgy* B 124, 147-174. doi:10.1179/1743275815Y.0000000014

Powell, R., Evans, K.A., Green, E.C.R., White, R.W., 2018. On equilibrium in non-hydrostatic metamorphic systems. *Journal of Metamorphic Geology* 36, 419–438. doi:10.1111/jmg.12298

Rabinowicz, M., Vigneresse, J.L., 2004. Melt segregation under compaction and shear channeling: Application to granitic magma segregation in a continental crust. *Journal of Geophysical Research* B109, B04407. doi:10.1029/2002JB002372

Rey, P., Müller, R. (2010). Fragmentation of active continental plate margins owing to the buoyancy of the mantle wedge. *Nature Geoscience* 3, 257–261. doi:10.1038/ngeo825

Rittner, M., Vermeesch, P., Carter, A., Bird, A., Stevens, T., Garzanti, E., Ando, S., Vezzoli, G., Dutt, R., Xu, Z., Lu, H., 2016. The provenance of Taklamakan desert sand. *Earth and Planetary Science Letters* 437, 127-137. doi:10.1016/j.epsl.2015.12.036

Rushmer, T., 2001. Volume change during partial melting reactions: implications for melt extraction, melt geochemistry and crustal rheology. *Tectonophysics* 342, 389-405. doi:10.1016/S0040-1951(01)00172-X

Sawyer, E.W., 1998. Formation and evolution of granite magmas during crustal reworking: the significance of diatexites. *Journal of Petrology* 39, 1147-1167. doi:10.1093/petroj/39.6.1147

Sawyer, E.W., 2008. *Atlas of migmatites*. NRC Research Press 387 pp.

Sawyer, E.W., 2020. Petrogenesis of secondary diatexites and the melt budget for crustal reworking, *Journal of Petrology* 61, egaa039, doi:10.1093/petrology/egaa039

Schorn, S., 2018. Dehydration of metapelites during high-P metamorphism: The coupling between fluid sources and fluid sinks. *Journal of Metamorphic Geology* 36, 369-391. doi:10.1111/jmg.12296

Schorn, S., Diener, J., Powell, R., Stüwe, K., 2018. Thermal buffering in the orogenic crust. *Geology* 46, 643-646. doi:10.1130/G40246.1

Skjerlie, K.P., Johnston, A.D., 1992. Vapor-absent melting at 10 kbar of a biotite- and amphibole-bearing tonalitic gneiss: Implications for the generation of A-type granites. *Geology* 20, 263-266. doi:10.1130/0091-7613(1992)020<0263:VAMAKO>2.3.CO;2

Stüwe, K., 1997. Effective bulk composition changes due to cooling: a model predicting complexities in retrograde reaction textures. *Contributions to Mineralogy and Petrology* 129, 43–52. doi:10.1007/s004100050322

Tarling, M.S., Smith, S.A.F., Scott, J.M., 2019. Fluid overpressure from chemical reactions in serpentinite within the source region of deep episodic tremor. *Nature Geoscience* 12, 1034–1042. doi:10.1038/s41561-019-0470-z

Taylor, S.R., McLennan, S.M., 1985. *The Continental Crust: Its Composition and Evolution.* Blackwell, 328 pp.

Taylor, S.R., McLennan, S.M., 1995. The geochemical evolution of the continental crust. *Reviews in Geophysics* 32, 241-265. doi:10.1029/95RG00262

Vigneresse, J.L, Barbey, P., Cuney, M., 1996. Rheological transitions during partial melting and crystallization with application to felsic magma segregation and transfer. *Journal of Petrology* 37, 1597-1600. doi:10.1093/petrology/37.6.1579

Vigneresse, J.L, Burg, J.P., 2005. Simulation of crustal melt segregation through cellular automata: Insight on steady and non-steady state effects under deformation. *Pageoph* 162, 987-1011. doi:10.1007/s00024-004-2652-9

Vigneresse, J.L., Burg, J.P., 2000. Stable continuous versus discontinuous melt segregation in migmatites. *Terra Nova* 12, 188-192. doi:10.1046/j.1365-3121.2000.00299.x

Vigneresse, J.L., Truche, L., 2020. Modeling ore generation in a magmatic context. *Ore Geology Reviews* 116, 103223. doi:10.1016/j.oregeorev.2019.103223

Wang, W., Clarke, G., Daczko, N., Zhao, Y. 2019. Modelling the partial melting of metasediments in a low-pressure regional contact aureole: The effect of water and whole-rock composition. *Geological Magazine, 156,* 1400-1424. doi:10.1017/S001675681800078X

Ward, R., Stevens, G., Kisters, A., 2008. Fluid and deformation induced partial melting and melt volumes in low-temperature granulite-facies metasediments, Damara Belt, Namibia. *Lithos* 105, 253-27. doi:10.1016/j.lithos.2008.04.001

Wei, C., Powell, R., 2006. Calculated phase relations in the system NCKFMASH (Na_2O–CaO–K_2O–FeO–MgO–Al_2O_3–SiO_2–H_2O) for high-pressure metapelites. *Journal of Petrology* 47, 385-408. doi:10.1093/petrology/egi079

Weinberg, R.F., Hasalová, P., 2015. Water-fluxed melting of the continental crust: A review. *Lithos* 212-215, 158-188. doi:10.1016/j.lithos.2014.08.021

Weinberg, R.F., Hasalová, P., Ward, L.K., Fanning, C.M., 2013. Interaction between deformation and magma extraction in migmatites: Examples from Kangaroo Island, South Australia. *Geological Society of America Bulletin* 125, 1282-1300. doi:10.1130/B30781.1

Weltje, G.J., 2002. Quantitative analysis of detrital modes: statistically rigorous confidence regions in ternary diagrams and their use in sedimentary petrology. *Earth-Science Reviews* 57, 211-253. doi:10.1016/S0012-8252(01)00076-9

Weltje, G.J., 2012. Quantitative models of sediment generation and provenance: State of the art and future developments. *Sedimentary Geology* 280, 4-20. doi:10.1016/j.sedgeo.2012.03.010

White, R.W., Powell, R, Holland, T.J.B., 2001. Calculation of partial melting equilibria in the system Na_2O–CaO–K_2O–FeO–MgO–Al_2O_3–SiO_2–H_2O (NCKFMASH). *Journal of Metamorphic Geology* 19, 139-153. doi:10.1046/j.0263-4929.2000.00303.x

White, R.W., Powell, R., Halpin, J.A., 2004. Spatially-focussed melt formation in aluminous metapelites from Broken Hill, Australia: *Journal of Metamorphic Geology* 22, 825-845. doi:10.1111/j.1525-1314.2004.00553.x

White, R.W., Powell, R., Holland, T.J.B., 2007, Progress relating to calculation of partial melting equilibria for metapelites. *Journal of Metamorphic Geology* 25: 511-527. doi:10.1111/j.1525-1314.2007.00711.x

Wolf, M., Wyllie, P.J., 1991. Dehydration-melting of solid amphibolite at 10 kbar: Textural development, liquid interconnectivity and applications to the segregation of magmas. *Mineralogy and Petrology* 44, 151-179. doi:10.1007/BF01166961

FIGURE CAPTIONS

Figure 1. Pressure-Temperature grid illustrating three cases of melting, with the starting point represented by a plain circle. A clockwise path (CW in yellow) in which pressure increases due to crustal thickening and induced temperature increase. Two paths describe CCW paths with decompression melting from low (light blue) and high pressure (heavy blue) domains. Kyanite (ky), andalusite (and) and sillimanite (sil) domains and the triple point rare indicated as a reference. Melting curves with (plain line) and without water (dashed lines) are also represented for muscovite and biotite dehydration melting. The fields of greenschist (gf), blueschist (bf), amphibolite (af), eclogite (ef), migmatite (mf) and granulite facies (γf) are also represented.

Figure 2. Binary melting with quartz and muscovite, and plagioclase, obtained from Eq.1. Results are indicated in melt volume %, indicating the changes in proportion when muscovite or quartz runs out first.

Figure 3. Melt fertility as a function of original Qtz, Ms and Bt content, with Pl considered in excess. Muscovite dehydration melting (1), followed by Bt dehydration melting (2). Equations (1) and (2) were used (see text). The melt is represented in volume %. Note the changes when Ms, Kfs or Qtz run out first during muscovite dehydration, or when Bt, Sil or Qtz run out during biotite dehydration.

Figure 4. Quartz – Feldspar – Lithic fragments (QFL) ternary diagrams, showing the amount of quartz, feldspathic and lithic (micas) minerals, according to three tectonic settings of crustal melting. The products of eolian erosion of continental basement (CB) contain a larger quartz amount. Fluvial erosion involves older sediments, resulting in more mudstones and sandstones during orogen recycling (OR). The products of magmatic arc evolution (MA) contain more micas resulting from volcanic activity. The three identified paths are indicated, and minerals are discriminated according to their tectonic origin. A discrimination between feldspars and micas is also reported in the three sedimentary settings.

Figure 5. Schematic representation of minerals melting, using an Eulerian and a Lagrangian description. In the first case, the lines of descent separate two domains in which two types of crystals (M1 and M2) coexist with melt. Each phase must be represented with its composition and relevant physical parameters (e.g. viscosity) as a function of temperature. Conversely, the Lagrangian description only considers the phases in presence (liquid or crystalline M). But the textural location of each phase is not considered.

Figure 6. Melt production as a function of their textural distribution, and according to the chemical equation of dehydration. Two thresholds control liquid percolation (LPT), i.e. melt motion, and melt extraction (MET). The various textural configurations include random (r), layered(l) or clustered minerals (c). Two types of particles motion under pure shear (PS) or simple shear (SS) modify the disposition of cell. The removal of the melt may occur when several cells containing melt allow its motion under strain. The melting equation is from eq. 3, after normalization by a factor 8 to get round mole values.

Figure 7. Melt productivity according to the textural disposition in thin (top) or thick (bottom) layers. Thick layers, i.e. implying thickness larger than the usual mineral size, enhance the adequate minerals to be in contact for melting. The results are plotted onto a triangular QFL diagram (see text) representing quartz, feldspars and lithic (micas) composition.

Figure 8. Dynamic melt extraction modeling (Vigneresse and Burg, 2000; 2004) using a Lagrangian description. Here only the amount of segregated melt may be estimated, starting with a quantitative distribution of the initial melt. The amount of melt extracted follows a spiky distribution, that marks by stiction spikes when it is suddenly modified. A too large amount of melt, results in a stick-slip behavior with little highs and lows. Conversely, when the melt content is lower than its capacity to escape the system, a smoother amount of melt is observed. When normalized to the initial melt amount, the coefficient of melt extraction remains constant.

Figure 9. Effect of stress, pure shear (PS) and simple shear (SS) or both on the amount of melt extracted during successive cycles. Pure shear is more effective in extracting melt, whereas simple shear only displaces it laterally, along the sense of shear in 2D.

Figure 10. QFL diagram representing the sedimentary data used. Continental basement (CB) sandstones from Old Red Sandstones, NW Australia and Asian deserts are shown by squares.

Mudstones from African and Indus fans (diamonds) result from various compilations (Weltje, 2002; 2012; Garzanti, 2019). To this compilation, Amazon Indian and Bengal fan sediments (squares) corresponds to fluvial erosion (OR). Fluvial deposits from closed ocean (Mediterranean) are included as plain circles. In order to represent magmatic arcs domain (MA), sediments from the Pacific trench (Peru-Chile), from the west Pacific trench sediments (right triangles) and Asian trenches (left triangles) have been added (see text for the references). The respective melt productivity for each metasedimentary composition is also represented.

Figure 11. Detailing the respective content (in vol %) in plagioclase, K-feldspars and micas (biotite and muscovite) in a description using the QFL schema. As expected, the two former minerals concentrate toward the F pole, whereas micas are more abundant toward the L (lithic) pole. The distribution is linear in case of micas, but it follows a quadratic distribution for feldspars that are found in both arcs detritus and mudstones.

Figure 12. Effective melt productivity according to the origin of the metasediments. In case of continental basement recycling (CB), quartz excess strongly limits the amount of melt to less than 10 %. Orogenic recycling (OR) also shows quartz as the dominant mineral, but with more input from altered minerals, through mudstones, yielding an effective melt productivity below 40 %. The larger melt productivity, up to 55 % in rare cases, is observed in magmatic arc (MA) recycling, owing to the abundance in micas.

Table 1. Stoichiometric reactions (Rushmer, 2001) after normalization to 1 muscovite and 1 biotite. The total melt percentage and melt/mole are included.

Table 1. Stoichiometric reactions (Rushmer, 2001) after normalization to 1 muscovite and 1 biotite. The total melt percentage and melt/mole are included.

mus	bt	plag	qtz		bt	kspar	sil	opx	spl	cord	gar	Feox	melt	Σmole
1		0.320	0.360	→	0.090	0.220	0.220						1.140	1.680
	1	0.053	0.540	→		0.590		0.730	0.020				0.280	1.593
	1	0.130	0.550	→		0.390		0.615		0.017			0.630	1.680
	1	0.198	0.360	→		0.520		0.565			0.119		0.320	1.558
	1	0.159	1.114	→				0.230			0.160	0.068	1.727	2.273
	1	0.972	0.886	→				0.160			0.160	0.029	1.914	2.858

Highlights

- A numerical estimate of melt in metapelites
- Effective melt productivity as a function of texture
- Effective melt productivity as a function of composition of the protolith
- Discontinuous melt extraction in spite of continuous heating

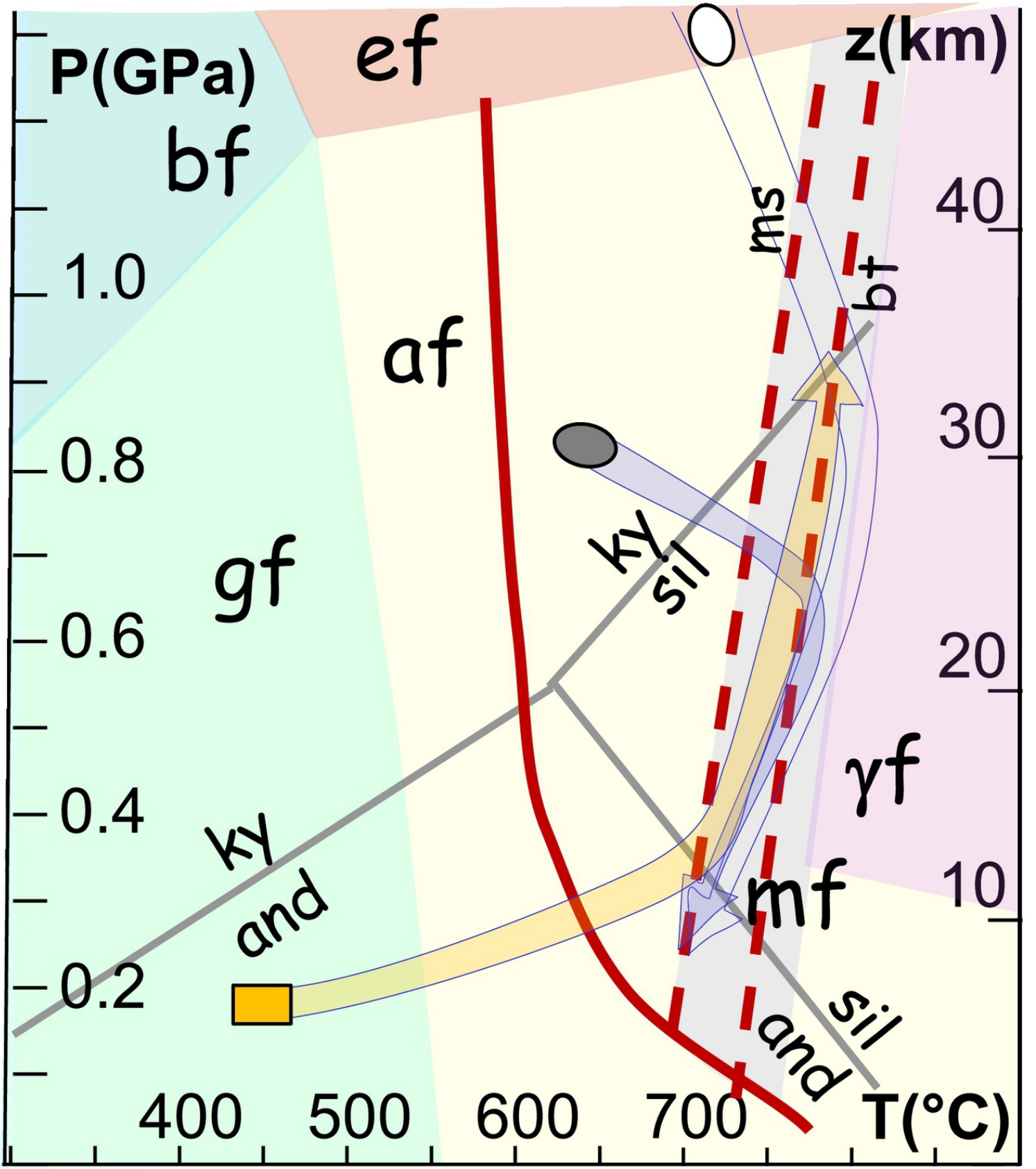
P(GPa)
z(km)
ef
bf
af
gf
γf
mf
ms
bt
ky
sil
and
1.0
0.8
0.6
0.4
0.2
40
30
20
10
400
500
600
700
T(°C)

Figure 1

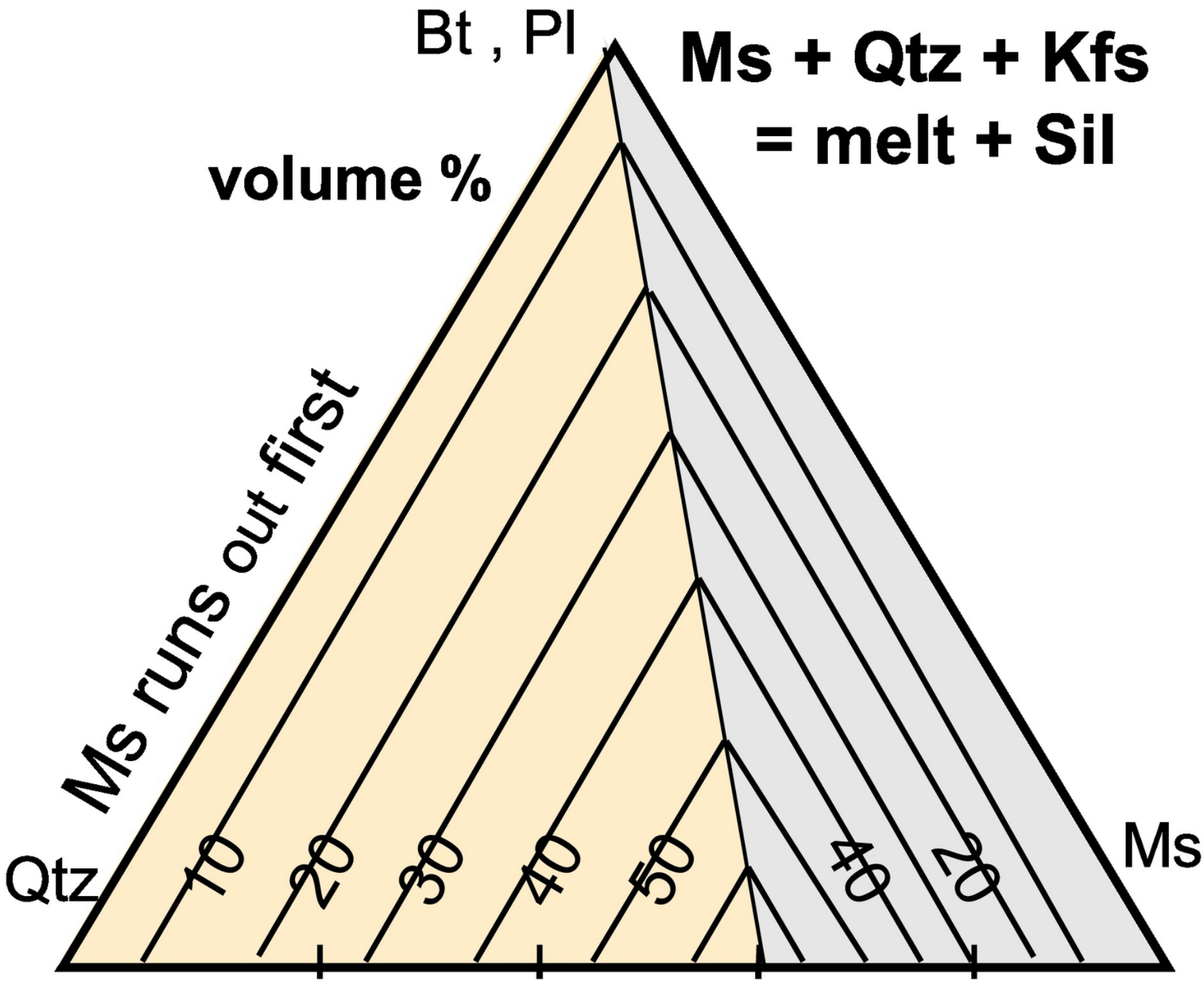
Bt , Pl
Ms + Qtz + Kfs
= melt + Sil
volume %
Ms runs out first
Qtz
Ms
10
20
30
40
50
40
20

Figure 2

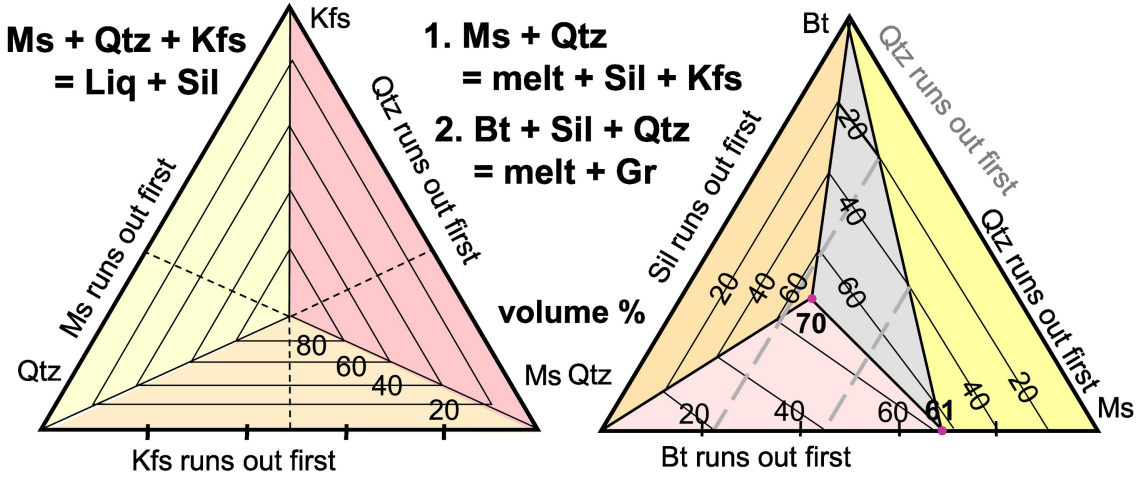
Ms + Qtz + Kfs
= Liq + Sil
Kfs
Qtz runs out first
Ms runs out first
Qtz
80
60
40
20
Kfs runs out first
1. Ms + Qtz
= melt + Sil + Kfs
2. Bt + Sil + Qtz
= melt + Gr
volume %
Ms Qtz
Bt
Qtz runs out first
Sil runs out first
Qtz runs out first
20
40
60
70
61
Ms
Bt runs out first

Figure 3

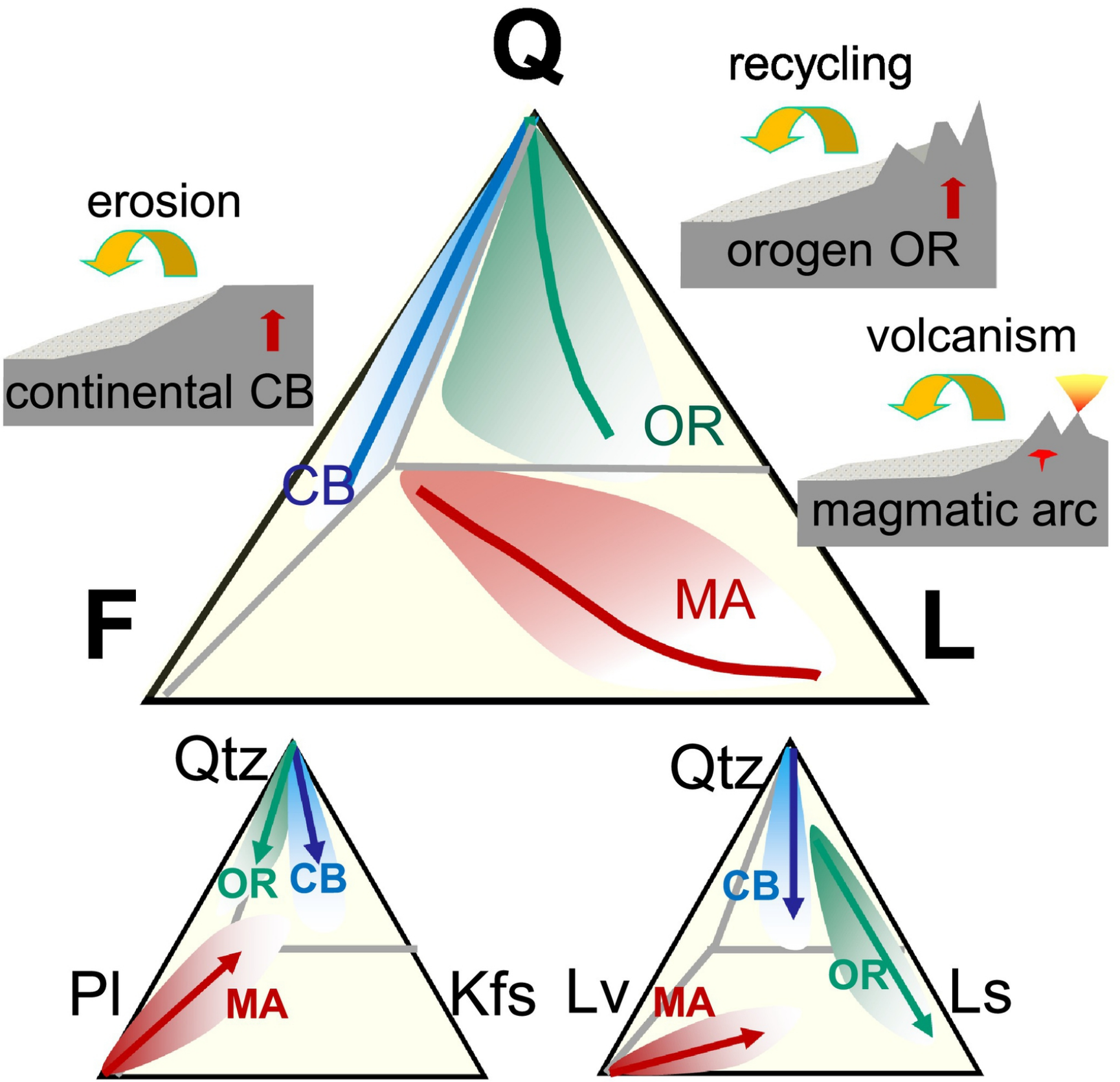
Q
recycling
orogen OR
erosion
continental CB
volcanism
magmatic arc
OR
CB
MA
F
L
Qtz
OR
CB
Pl
MA
Kfs
Qtz
CB
OR
Lv
MA
Ls

Figure 4

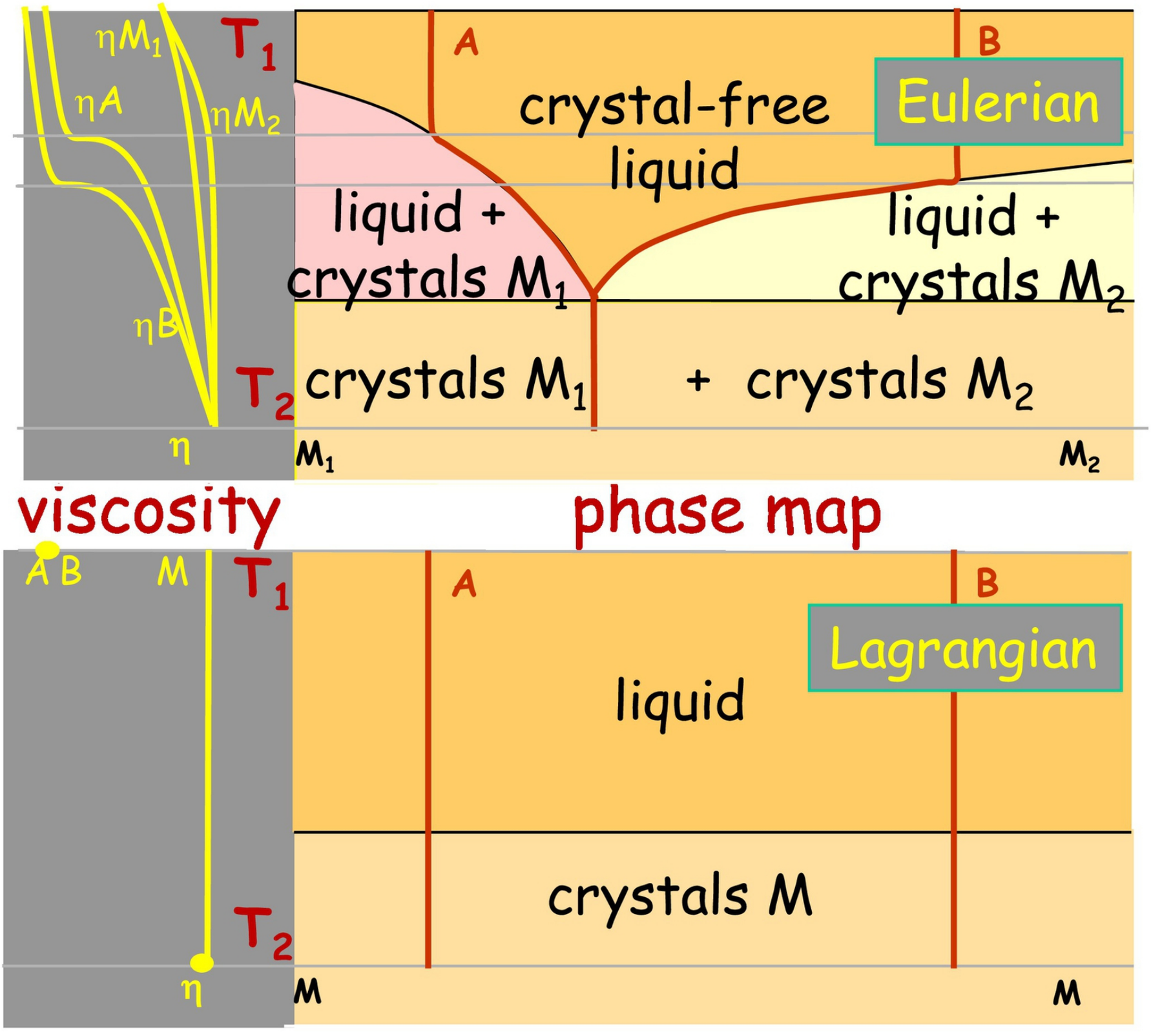
ηM1
T1
ηA
ηM2
ηB
T2
η
A
B
crystal-free
liquid
Eulerian
liquid +
crystals M1
liquid +
crystals M2
crystals M1
+ crystals M2
M1
M2
viscosity
phase map
A B
M
T1
T2
η
A
B
Lagrangian
liquid
crystals M
M
M

Figure 5

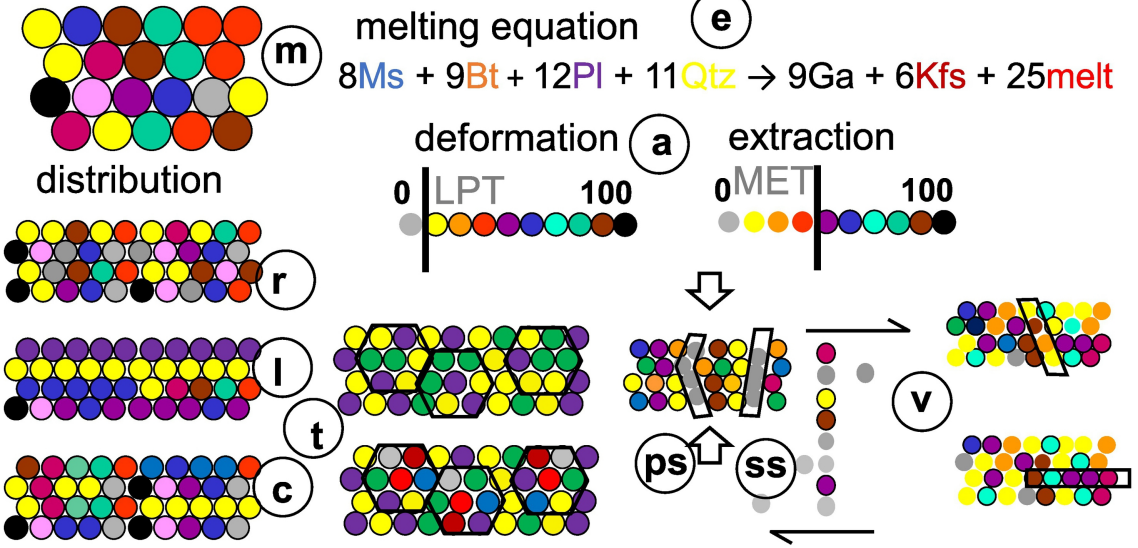
m
melting equation
e
8Ms + 9Bt + 12Pl + 11Qtz → 9Ga + 6Kfs + 25melt
deformation
a
extraction
0
LPT
100
0
MET
100
distribution
r
l
t
c
ps
ss
v

Figure 6

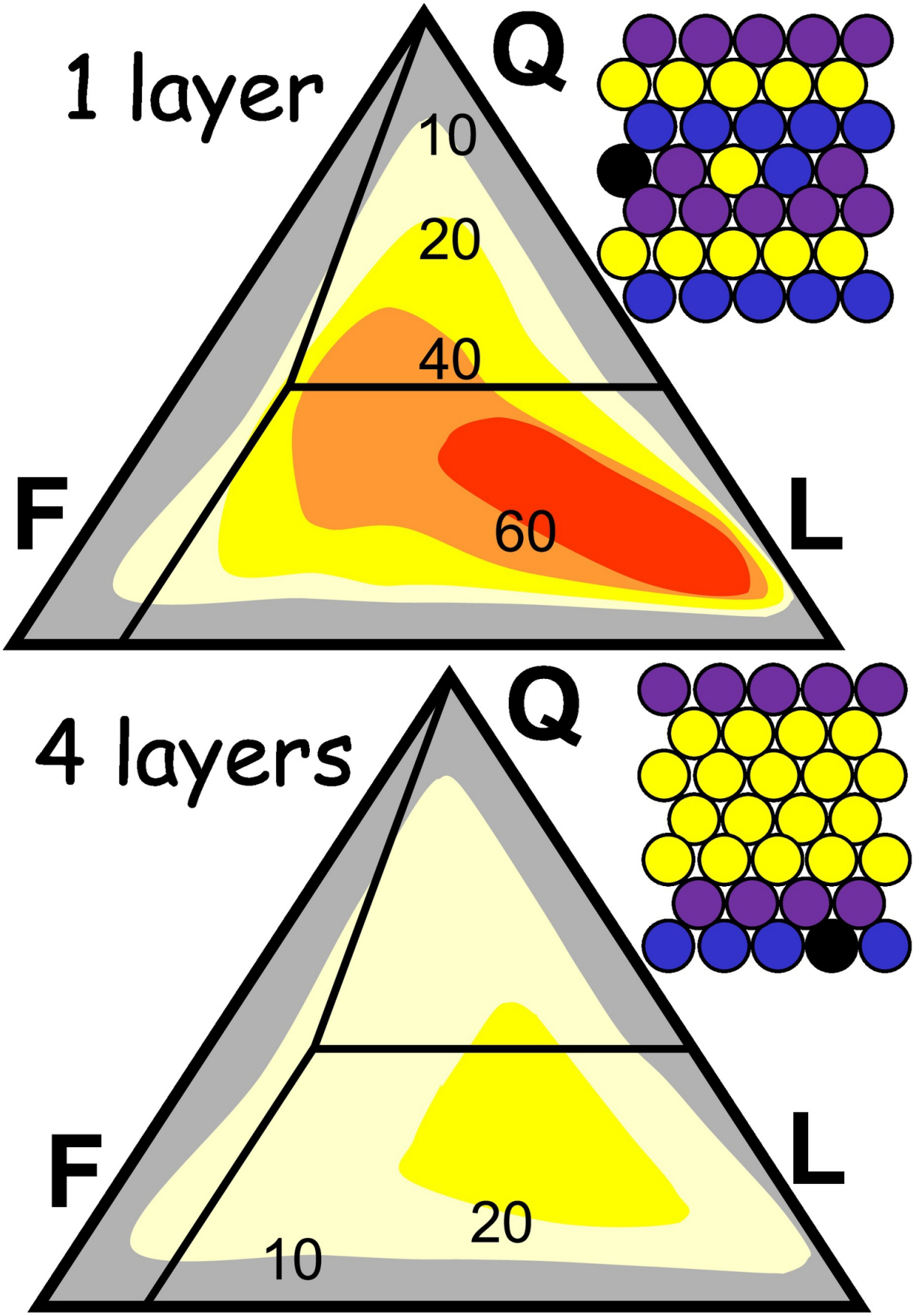

Figure 7

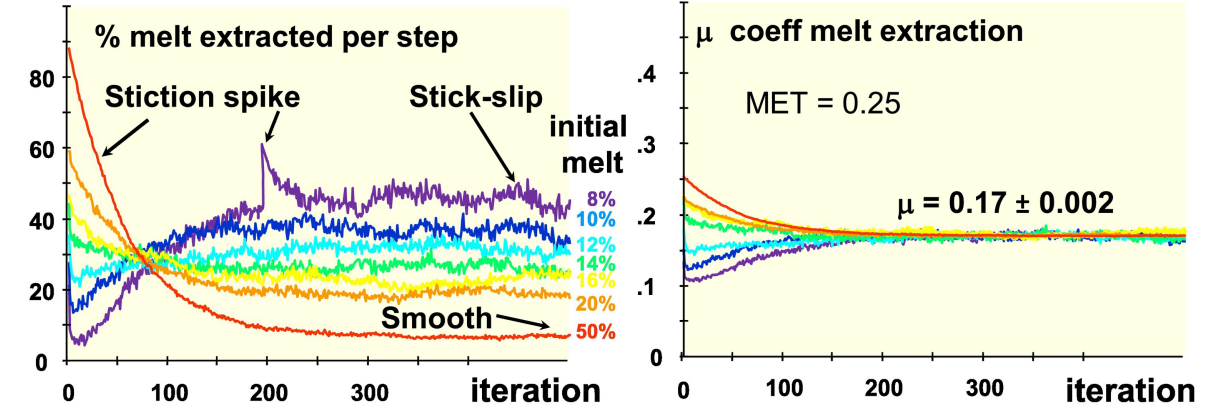
% melt extracted per step
Stiction spike
Stick-slip
initial melt
8%
10%
12%
14%
16%
20%
50%
Smooth
80
60
40
20
0
0
100
200
300
iteration
μ coeff melt extraction
MET = 0.25
μ = 0.17 ± 0.002
.4
.3
.2
.1
0
0
100
200
300
iteration

Figure 8

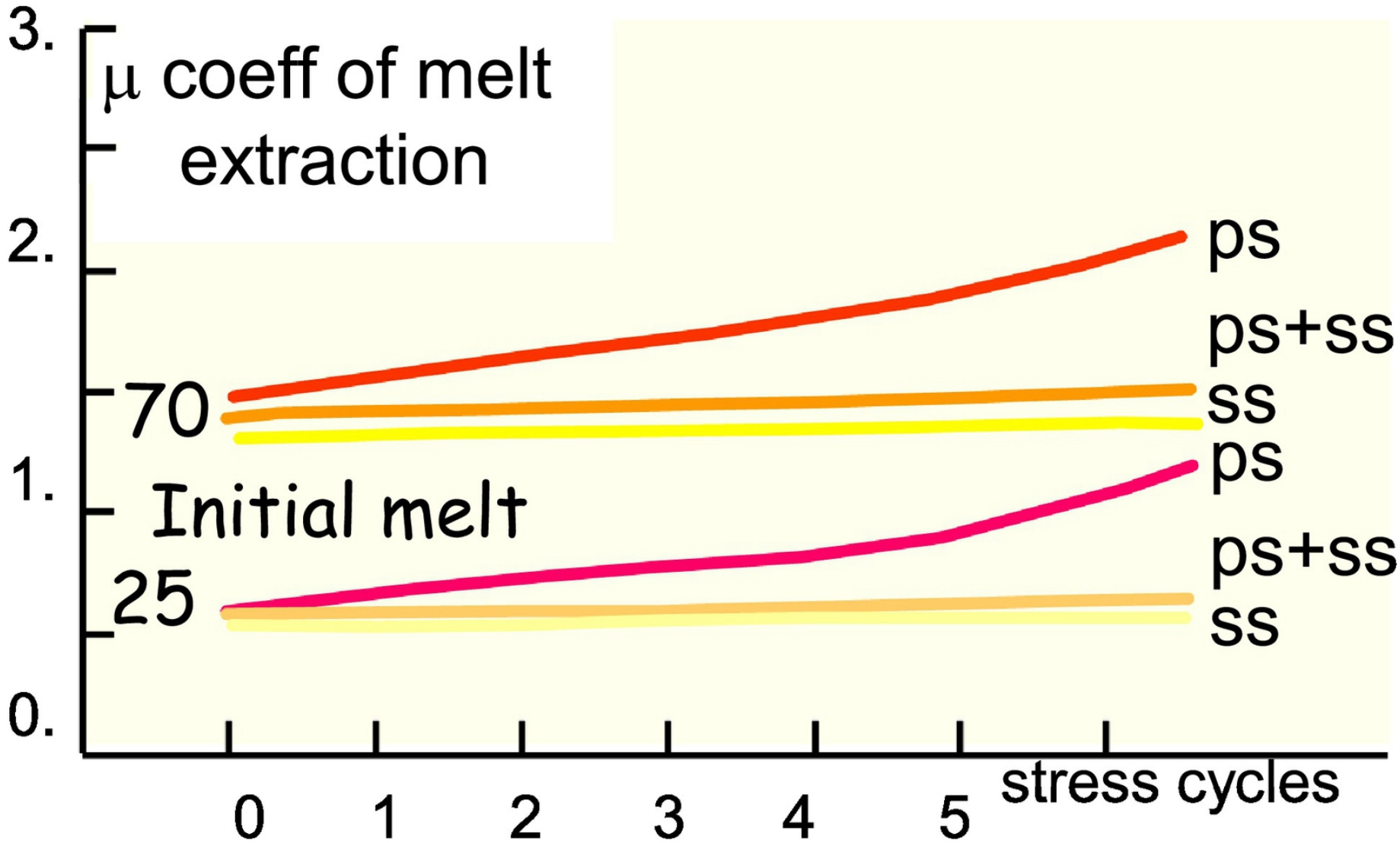
3.
μ coeff of melt
extraction
2.
70
1.
Initial melt
25
0.
ps
ps+ss
ss
ps
ps+ss
ss
0
1
2
3
4
5
stress cycles

Figure 9

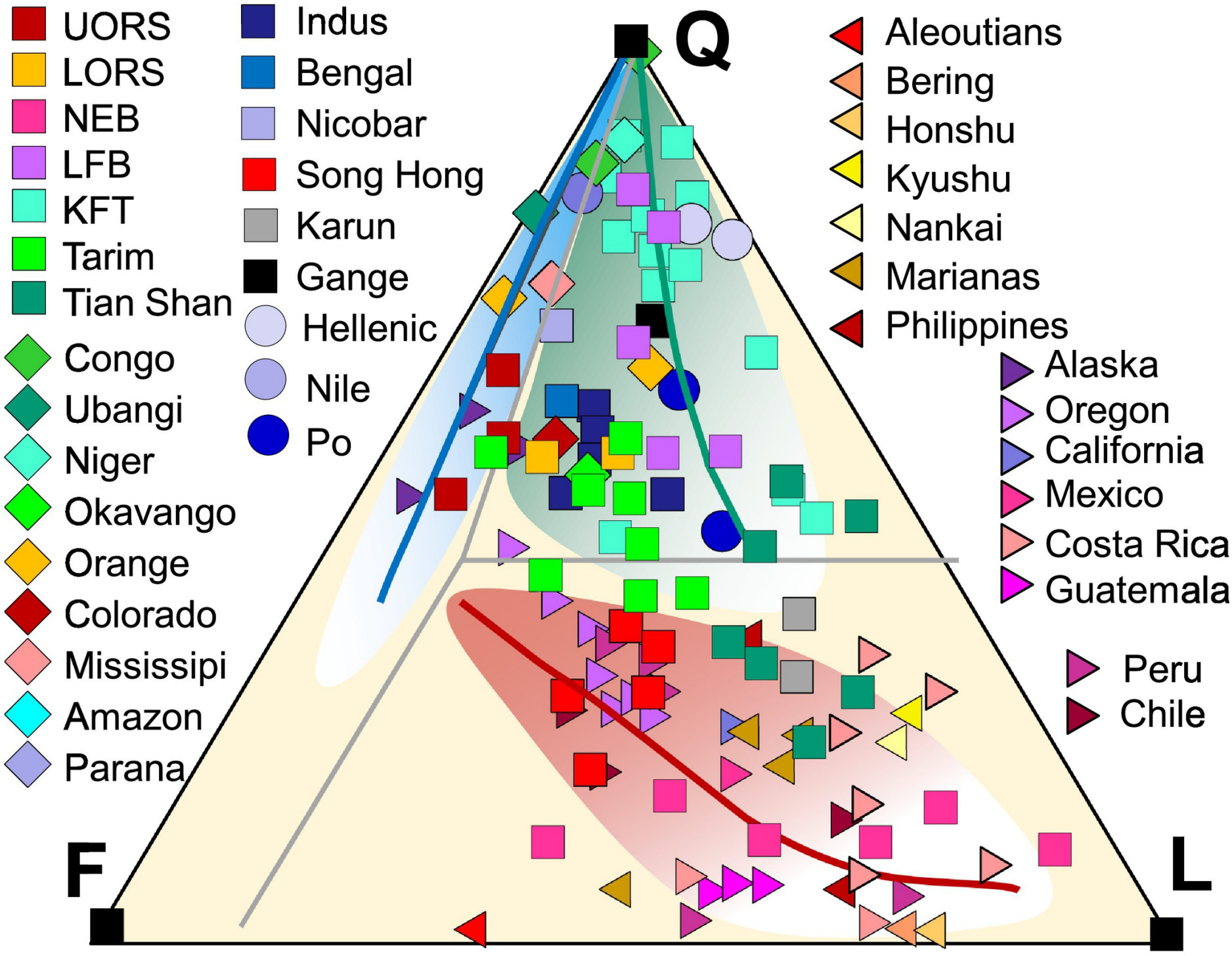
UORS
LORS
NEB
LFB
KFT
Tarim
Tian Shan
Congo
Ubangi
Niger
Okavango
Orange
Colorado
Mississipi
Amazon
Parana
Indus
Bengal
Nicobar
Song Hong
Karun
Gange
Hellenic
Nile
Po
Q
F
L
Aleoutians
Bering
Honshu
Kyushu
Nankai
Marianas
Philippines
Alaska
Oregon
California
Mexico
Costa Rica
Guatemala
Peru
Chile

Figure 10

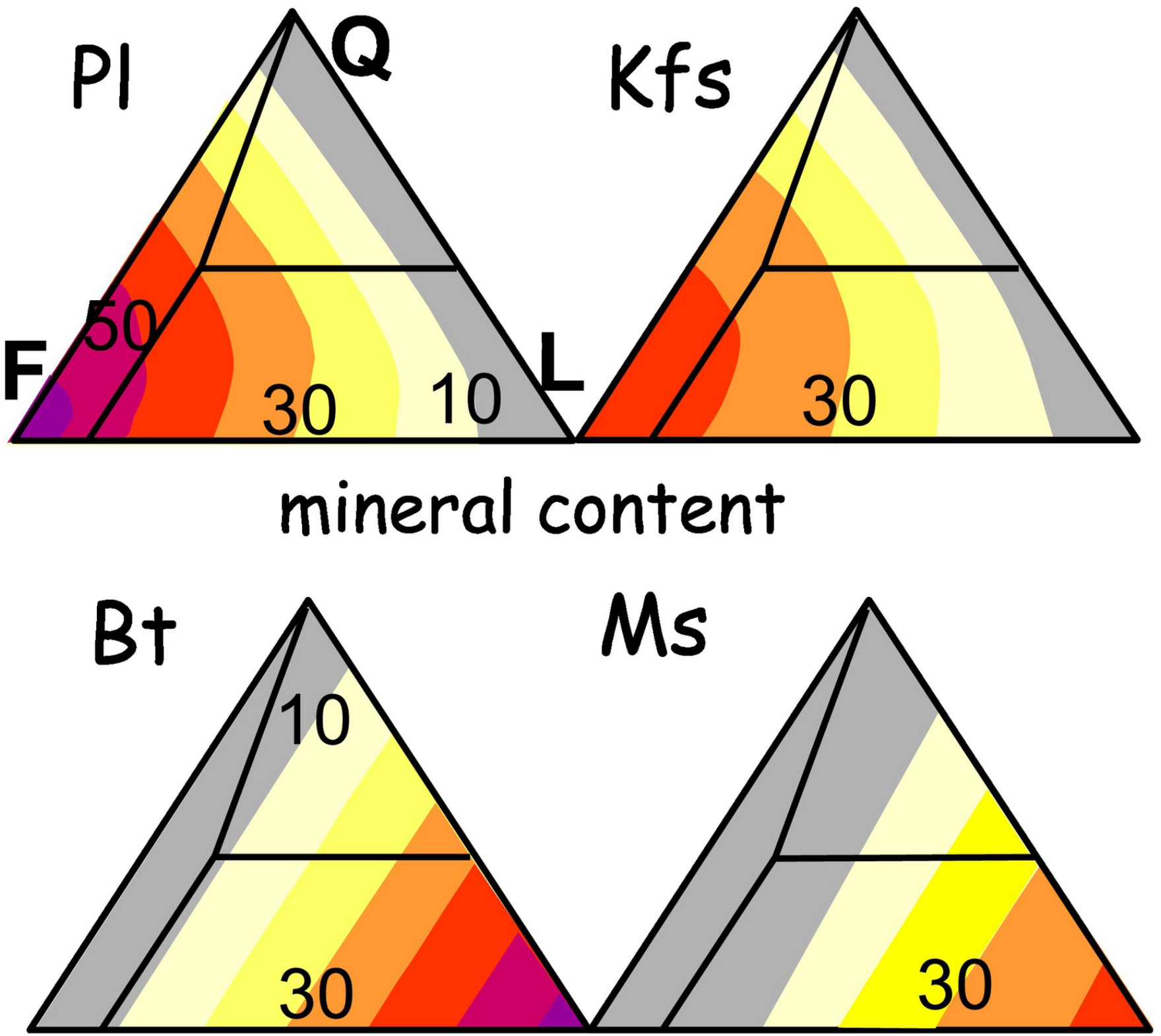

Figure 11

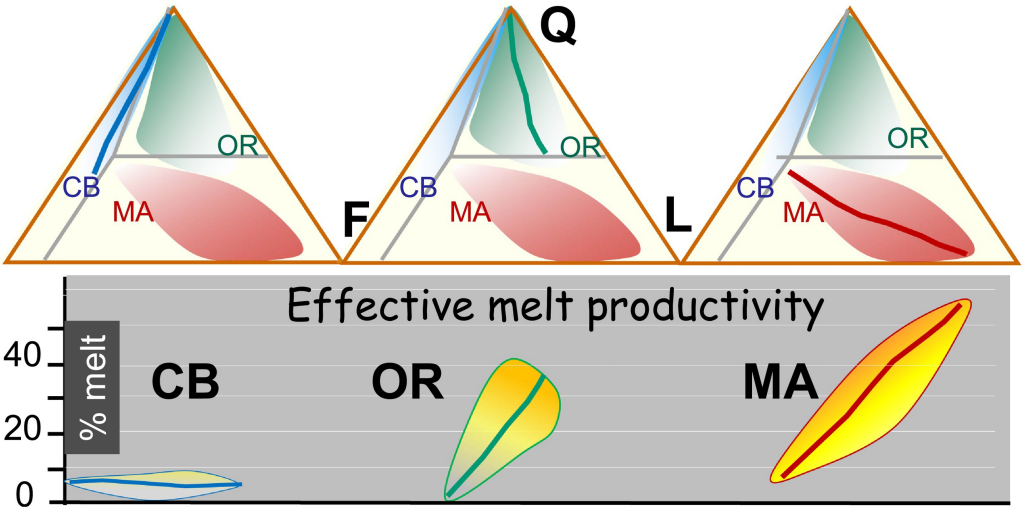
Q
F
L
CB
OR
MA
CB
OR
MA
CB
OR
MA
Effective melt productivity
% melt
40
20
0
CB
OR
MA

Figure 12